



HAL
open science

Biosynthesis of a broad-spectrum nicotianamine-like metallophore in *Staphylococcus aureus*

Ghassan Ghssein, Catherine Brutesco, Laurent Ouerdane, Clémentine Fojcik, Amélie Izaute, Shuanglong Wang, Christine Hajjar, Ryszard Lobinski, David Lemaire, Pierre Richaud, et al.

► **To cite this version:**

Ghassan Ghssein, Catherine Brutesco, Laurent Ouerdane, Clémentine Fojcik, Amélie Izaute, et al.. Biosynthesis of a broad-spectrum nicotianamine-like metallophore in *Staphylococcus aureus*. *Science*, 2016, 352 (6289), pp.1105-1109. 10.1126/science.aaf1018 . hal-03133612

HAL Id: hal-03133612

<https://hal.science/hal-03133612v1>

Submitted on 13 Feb 2021

HAL is a multi-disciplinary open access archive for the deposit and dissemination of scientific research documents, whether they are published or not. The documents may come from teaching and research institutions in France or abroad, or from public or private research centers.

L'archive ouverte pluridisciplinaire **HAL**, est destinée au dépôt et à la diffusion de documents scientifiques de niveau recherche, publiés ou non, émanant des établissements d'enseignement et de recherche français ou étrangers, des laboratoires publics ou privés.

1 **Title: Biosynthesis of a broad-spectrum nicotianamine-like metallophore in**
2 **Staphylococcus aureus**

3
4 **Authors:** Ghassan Ghssein^{1,2,3,*}, Catherine Brutesco^{1,2,3,*}, Laurent Ouerdane^{4,*}, Clémentine
5 Fojcik⁵, Amélie Izaute^{1,2,3}, Shuanglong Wang⁴, Christine Hajjar^{1,2,3}, Ryszard Lobinski⁴, David
6 Lemaire^{2,3,6}, Pierre Richaud^{2,3,7}, Romé Voulhoux⁸, Akbar Espaillat⁹, Felipe Cava⁹, David
7 Pignol^{1,2,3}, Elise Borezée-Durant⁵, Pascal Arnoux^{1,2,3,†}

8 **Affiliations:**

9 ¹CEA, DSV, IBEB, Laboratoire de Bioénergétique Cellulaire, Saint-Paul-lez-Durance, France

10 ²CNRS, UMR 7265 Biologie Végétale et Microbiologie Environnementales, Saint-Paul-lez-
11 Durance, France-

12 ³Aix Marseille Université, CEA, CNRS, BVME UMR 7265, 13108, Saint Paul-Lez-Durance,
13 France

14 ⁴CNRS-UPPA, Laboratoire de Chimie Analytique Bio-inorganique et Environnement,
15 UMR5254, Hélioparc, 2, Av. Angot, 64053 Pau, France

16 ⁵Micalis Institute, INRA, AgroParisTech, Université Paris-Saclay, 78350 Jouy-en-Josas, France

17 ⁶CEA, DSV, IBEB, Lab Interact Protein Metal, Saint-Paul-lez-Durance, France

18 ⁷CEA, DSV, IBEB, Lab Bioenerget Biotechnol Bacteries & Microalgues, Saint-Paul-lez-
19 Durance, France

20 ⁸CNRS & Aix-Marseille Université, Laboratoire d'Ingénierie des Systèmes Macromoléculaires
21 (UMR7255), Institut de Microbiologie de la Méditerranée (IMM), Marseille, France

22 ⁹Laboratory for Molecular Infection Medicine Sweden, Department of Molecular Biology, Umeå
23 Centre for Microbial Research, Umeå University, Umeå, Sweden

24
25 *These authors contributed equally to this work.

26 †Correspondence to: pascal.arnoux@cea.fr.
27

1 **Abstract:** Metal acquisition is a vital microbial process in metal-scarce environments such as
2 inside a host. Using metabolomic exploration, targeted mutagenesis, and biochemical analysis,
3 we discovered an operon in *Staphylococcus aureus* that encodes the different functions required
4 for the biosynthesis and trafficking of a broad-spectrum metallophore related to plant
5 nicotianamine (here called staphylopine). The biosynthesis of staphylopine reveals the
6 association of three enzyme activities: a histidine racemase, an enzyme distantly related to
7 nicotianamine synthase, and a staphylopine dehydrogenase belonging to the DUF2338 family.
8 Staphylopine is involved in nickel, cobalt, zinc, copper and iron acquisition, depending on the
9 growth conditions. This biosynthetic pathway is conserved across other pathogens, thus
10 underscoring the importance of this metal acquisition strategy in infection.

11

12

1 **Main Text:**

2 Metals are required in many life processes and, consequently, all organisms have
3 developed mechanisms for their uptake and homeostasis. Pathogenic bacteria must face an
4 additional barrier of metal limitation that is usually set by the host, precisely in order to prevent
5 bacterial growth (1). This strategy of “nutritional immunity” by the hosts also extends to many
6 micronutrients such as iron, manganese or zinc with dedicated mechanisms of sequestration (2,
7 3). The paradigm of metal acquisition in metal-deprived environments is associated with iron:
8 whereas one strategy consists in transporting the reduced form, the most common scheme
9 involves the synthesis of high affinity ferric siderophores, their extracellular release prior to
10 capture and import of the siderophore-Fe³⁺ complex (4). These siderophores are frequently
11 associated with virulence and may also be used for the transport of metals other than iron (5, 6),
12 with only a few examples of other types of microbial metallophores. Methanobactin, for
13 example, is a peptide-based chalkophore used for copper scavenging by methane oxidizing
14 bacteria (7). Free L-Histidine is used as a nickelophore by some bacteria, and more complex
15 molecules are possibly used by *S. aureus* or *H. pylori*, although their identity or functional
16 relevance are unknown (8, 9). Recently, a nickel/cobalt uptake system (called CntA-F) was
17 uncovered in *S. aureus* and was found to play a role in the virulence of this strain (10).

18 Plants have also evolved their own metal chelators and among them, nicotianamine is an
19 important metabolite that is essential in the homeostasis of iron, copper, nickel and zinc (11, 12).
20 Nicotianamine is also the first precursor of phytosiderophores, a family of molecules chemically
21 different but functionally equivalent to siderophores (13). Nicotianamine is enzymatically
22 synthesized by nicotianamine synthase (NAS), which catalyzes the condensation of three α -
23 aminobutyric acid moieties from S-adenosylmethionine (SAM) with the cyclization of one of
24 them to form an azetidone ring (14-16). Nicotianamine and its phytosiderophore derivatives seem
25 to be restricted to plants and some fungi, although some archaea apparently produce a
26 nicotianamine-related molecule called thermonicotianamine, of which the functional role
27 remains unknown (17).

28 Trying to better understand this family of plant NAS and archaeal NAS-like enzymes, we
29 found a gene putatively coding for a NAS-like enzyme in bacterial genome, including *S. aureus*.
30 The NAS-Like gene from *S. aureus* (*sav2469*), here called *cntL*, shares 12% sequence identity
31 with one of the four NAS from *Arabidopsis thaliana*, which corresponds to a very distant
32 homology. However, threading-based structure prediction programs detected a structural
33 homology of CntL with eukaryotic NAS and archaeal NAS-like enzymes (Fig. S1). The gene
34 coding for CntL is systematically located upstream of a gene whose product belongs to the
35 DUF2338 family (*cntM* in *S. aureus*, *sav2468*; Figs. 1, S2). Threading-based prediction indicates
36 with high confidence that this family of protein is related to Octopine-dehydrogenase, a
37 NAD(P)H dependent enzyme which reductively condensates a free amino acid, such as arginine,
38 with an α -ketoacid, such as pyruvate (18). This family of enzymes is known to be involved in the
39 escape of scallops from their starfish predators (19), or in the growth of parasitic bacteria, such
40 as *Agrobacterium tumefaciens* at the expense of plants in which they induce opine-producing
41 tumors, offering bacteria a selective growth advantage (20). In *S. aureus*, the gene upstream of
42 *cntL* (*cntK*, *sav2470*) appears restricted to the phylum of Firmicutes and encodes a protein that is
43 distantly related to a diaminopyrimidate epimerase (DapF).

1 On the basis of these predictions, the putative activity of each of these three enzymes
2 could be joined together to form a biosynthetic machinery: the CntK epimerase would produce
3 an amine substrate of proper stereochemistry that would be modified by the CntL NAS-like
4 enzyme through addition of one or two α -aminobutyric acid moiety(ies), and CntM would
5 reductively condensate an α -ketoacid to the previously formed product, leading to the formation
6 of a candidate molecule. Although their putative activity was not recognized at the time, the
7 three corresponding genes (*cntKLM*) were shown to belong to an operonic structure involved in
8 the import of nickel and cobalt ions through an ABC transporter named *cntA-F* (8, Fig. 1A). Two
9 independent genetic studies targeting either the solute binding protein (SBP; *cntA*) or the MFS
10 transporter (Major Facilitator Superfamily, here called *cntE*) indicated that this operon is
11 important for the virulence and fitness of *S. aureus* (10, 21). The phenotype of these mutations
12 could be reconciled by the hypothesis of a siderophore-like system with a biosynthetic
13 machinery (CntKLM), a putative exporter (CntE) and a putative importer of a metal-
14 metallophore complex (CntABCDF).

15 We attempted to identify the candidate metallophore through an *ab-initio* approach using
16 *E. coli* or *S. aureus* strains, and through a knowledge-based approach using purified proteins
17 (22). For the first approach we cloned the entire 10 kb *cnt* operon (*cntKLMABCDFE*) in *E. coli*
18 and induced gene expression and protein production. After adding nickel we tracked small
19 molecules co-eluting with nickel by metabolomic studies using hydrophilic interaction liquid
20 chromatography (HILIC; Fig. S3). We also constructed a mutant strain of *S. aureus* devoid of the
21 *cntL* gene and cultivated both the WT and this mutant strains in chemically defined media
22 (CDM), a media with low metal concentration in which expression of the operon is known (10).
23 We then detected metal complexes in the extracellular fractions by coupling HILIC separation
24 with inductively coupled plasma-mass spectrometry (ICP-MS) and electrospray ionization-mass
25 spectrometry (ESI-MS) (Fig. 1). A main peak was found to elute between 30 to 33 min in the
26 HILIC/ICP-MS experiment, with the retention time depending on the detected metal (Fig. 1B).
27 In all the cases these peaks were absent in the *cntL* mutant strain, therefore corroborating our
28 central hypothesis of the existence of a direct link between these metal complexes and the central
29 NAS-like enzyme. Investigation of these metal complexes by coupling HILIC and ESI-MS led
30 us to find a candidate molecule showing the characteristic metal isotopic patterns (Fig. 1C, Fig.
31 S3). The retention times of these compounds in HILIC/ESI-MS match those of the metals elution
32 found by HILIC/ICP-MS, therefore indicating that the same metal complexes were observed by
33 the two techniques. The knowledge-based approach consisted in the “fishing” of the nickel-
34 metallophore complex: we expressed and purified the SBP (CntA) from *E. coli* and incubated it
35 in a supernatant of a *cntA* mutant of *S. aureus* grown in CDM media. We then supplemented this
36 mix with nickel to force nickel-metallophore complex formation and binding to CntA. After re-
37 purification of the SBP and further analysis by MS we looked for the characteristic nickel
38 isotopic pattern and found a candidate molecule with the same mass as found by the
39 metabolomic approaches (Fig. S4). Using our set of accurate masses with molecular formula
40 finder softwares we proposed an empiric formula of $C_{13}H_{19}N_4O_6$ -Metal.

41 We attempted to fit this formula by using simple rules derived from our proposed
42 enzymes activities and putative substrates (22), and we finally propose the structure of a
43 candidate molecule that would be the result of three biosynthetic enzyme activities: 1)
44 racemization of L-histidine in D-histidine by CntK, 2) nucleophilic attack of one α -
45 aminobutyric acid moiety from SAM onto D-histidine to produce an intermediate (noted xNA)

1 by CntL and, 3) reductive condensation of the xNA intermediate with a molecule of pyruvate by
2 CntM (Fig. 2A). Gas-phase fragmentation of zinc and nickel metal complexes confirmed the
3 proposed structure of the discovered molecule (Fig. S5), which we name staphylopin to recall
4 its origin in *S. aureus* and its inclusion in the opine family (23).

5 We then tested and refined this hypothetical biosynthetic pathway by cloning, expressing
6 and purifying the three enzymes and by testing their respective activities (Figs. 2B-D, S6). First,
7 we incubated CntK with L- or D-histidine and found that it indeed produces D-histidine from the
8 L- stereoisomer and *vice versa*, therefore establishing CntK as a histidine racemase (Fig. 2B).
9 Because co-incubation with L-histidine and competing concentration of either L-alanine or L-
10 methionine did not inhibit the histidine racemase activity, CntK appears specific for histidine
11 (Fig. S7). CntK is therefore not a diaminopimelate epimerase as its sequence similarity could
12 suggest, but rather represents a novel enzyme family of histidine racemase. With regard to CntL
13 we determined a dissociation constant of 68 μM for SAM, which corroborates our central
14 hypothesis that CntL binds to SAM (Fig. S8). We then tested our prediction suggesting the
15 binding of NAD(P)H to CntM by incubating either NADH or NADPH with the purified enzyme.
16 This indicated a preference of the enzyme for NADPH, and fluorescence Resonance Energy
17 Transfer (FRET) between the tryptophan residue of the protein (excitation 280 nm, emission 340
18 nm) and NAD(P)H (340nm and 460 nm, respectively) further revealed that CntM is specific for
19 NADPH with a dissociation constant of about 50 μM (Fig. 2C), a value that was confirmed using
20 microcalorimetric titrations (Fig. S8). Therefore, CntM has the biochemical characteristics of
21 members of the opine synthase enzyme family, as suggested by the results of threading
22 programs.

23 We then investigated the combined enzymatic activities of CntK, CntL and CntM
24 through the use of a carboxyl- ^{14}C labeled SAM substrate. The use of this radiolabelled
25 substrate allowed us to follow the α -aminobutyric acid moiety of SAM after product separation
26 by thin layer chromatography (TLC) and autoradiography. We found that ^{14}C -labeled SAM
27 alone gave one strong band with three bands of lower intensity, likely corresponding to SAM and
28 some degradation products, such as, e.g. S-adenosyl-L-homocysteine (Fig. 2D). Interestingly,
29 although the incubation of ^{14}C -SAM with CntL and L-His did not change this SAM pattern, the
30 incubation with D-His led to a novel prominent band which migrated below the lowest SAM
31 band (Fig. 2D). According to our model, this band corresponds to the intermediate called xNA.
32 We then tested the effect of co-incubating both CntL and CntM enzymes together with their
33 putative substrates: L- and D-His, pyruvate and NADPH (Fig. 2D, lanes 4 and 5). Here again the
34 SAM pattern stayed unchanged using L-His. However, using D-His we could detect two novel
35 bands: one corresponding to the previous intermediate xNA, and one that migrated between the
36 two upper bands of SAM and would correspond to staphylopin. This identification is further
37 supported by the fact that the staphylopin band appears at the expense of the xNA intermediate,
38 as expected in such a case. We also confirmed the histidine racemase activity of CntK by co-
39 incubating all three enzymes together with their substrates. In this case, the incubation with L- or
40 D-His both led to the appearance of the xNA and staphylopin bands, in accordance with the
41 CntK activity, which produces both L- and D-His when supplied with either stereoisomer (Fig.
42 2D, lanes 6 and 7). Incubation of the three enzymes with different aminoacids, α -keto acids and
43 reducing agents confirms that the histidine racemase CntK is indeed specific for histidine and
44 that CntM could use neither NADH nor α -keto glutarate in place of NADPH and pyruvate,
45 respectively (Fig. S9). Overall, these *in vitro* studies of the three biosynthetic enzymes show that

1 they sequentially synthesize staphylopin according to our proposed scheme using common and
2 defined substrates.

3 Finally, we confirmed that staphylopin biosynthesis is impaired in the *cntL* mutant of *S.*
4 *aureus* and explored the effect of mutations of several genes in the *cnt* operon on metal
5 homeostasis and staphylopin production and trafficking (Fig. 3). When compared to WT strain
6 of *S. aureus*, both the xNA and the staphylopin bands disappeared in the *cntL* mutant,
7 confirming that both bands are dependent on CntL activity (Fig. 3A). Furthermore the bands
8 corresponding to xNA and staphylopin migrated at the same distance in *E. coli* or *S. aureus* cell
9 extracts, therefore confirming that both molecules are produced heterologously in *E. coli*. We
10 next sought to determine the effect of the *cntL* mutation with regard to intracellular metal
11 accumulation in various culture conditions: CDM, where metal concentration is rather low,
12 Chelex-demetalated CDM (dCDM) where metal level is even lower, NTA-demetalated CDM
13 supplemented with metalated NTA resin to supposedly mimic a chelating environment (rCDM),
14 and LB where metal concentration is high. We note that the growth of the *cntL* mutant is nearly
15 identical to that of the WT strain in these media (Fig. S10), therefore indicating that metal
16 content would be attributable to the absence of staphylopin and not to a growth defect. In all
17 these culture conditions we established that the *cnt* genes, transcribed from two promoters
18 upstream *cntKLM* and *cntA-E*, are highly expressed in metal scarce media, whereas their
19 activities is lower but still significant in LB (Fig. S11). In CDM and dCDM, the *cntL* mutation
20 caused a significant decrease in intracellular accumulation of nickel, copper and cobalt as
21 determined by ICP-MS (Figs. 3B, S12). This metal accumulation defect is comparable to the one
22 observed in the *cntA-F* mutant, indicating that metal or metal-staphylopin complexes are
23 transported *via* CntA (Fig. 3B). This defect in metal accumulation is complemented when
24 reintroducing the *cntL* gene in the mutant, although using slightly different conditions adapted
25 for ICP-AES metal content determination (Fig. S13). In this case there is no significant decrease
26 in intracellular copper, but a significant decrease in intracellular zinc, nickel and cobalt. In
27 rCDM, the tendency observed in CDM is confirmed, although in this condition iron, zinc,
28 copper, nickel and cobalt content are all affected in the mutant strain as compared to the WT.
29 Finally, in a metal rich medium such as LB, the *cntL* deletion mutant accumulated less iron,
30 copper and cobalt. Taken together, these sets of experiments suggest that, depending on the
31 nature of the metal, its concentration, and the bacterial growth status, staphylopin is involved in
32 the import of a large array of divalent metals in *S. aureus*. Testing metal transport over 10
33 minutes supports the involvement of both staphylopin and CntA-F in the import of all these
34 metals. Indeed, import of iron, zinc, nickel and cobalt are all significantly decreased in both *cntL*
35 and *cntA-F* mutants (Fig. 3C). The significant short-term transport of iron and zinc is consistent
36 with their known regulatory effect exerted on the *cnt* operon (10, 21). The transport of copper is
37 somehow different as WT cells efficiently export this metal during this short time, probably in
38 response to its toxicity. In this case the absence of CntL or CntA-F appears to decrease this
39 toxicity and its consecutive efflux. In order to investigate the transport of metal-staphylopin
40 complexes through CntA, we exploited the sensitivity of *S. aureus* to high cobalt concentration.
41 We found that *cntL* and *cntA-F* mutant strains are resistant to an otherwise toxic concentration of
42 cobalt to WT, whereas supplementation of synthetic staphylopin in the media restores its
43 toxicity in *cntL* but not in *cntA-F* strain (Fig. S14). This suggests a co-transport of cobalt-
44 staphylopin complexes *via* CntA-F, as the ABC transporter is still present in the *cntL* (hence the
45 cobalt toxicity) whereas it is absent in the *cntA-F* mutant (where cobalt-staphylopin cannot
46 enter the cell). Finally, we measured the staphylopin level in the intracellular and supernatant

1 fractions of the WT, *cntABCDF*, *cntL* and *cntE* mutants (Fig. 3D). This experiment confirmed
2 the absolute need of CntL in the biosynthesis of staphylopin, further supported the function of
3 CntA-F in the import of staphylopin-metal complexes, and clearly indicated that CntE is
4 involved in the export of staphylopin. Overall, despite being distantly related, staphylopin
5 apparently mirrors the effect that nicotianamine has on the same range of metal but in the context
6 of metal homeostasis and transport in plants (17). Chemically synthesized staphylopin has the
7 same range of metal affinity than nicotianamine (similar K_d and affinity order: $\text{Cu}^{2+} > \text{Ni}^{2+} >$
8 $\text{Co}^{2+} > \text{Zn}^{2+} > \text{Fe}^{2+}$; Fig. S15), further supporting their functional comparison as broad-spectrum
9 metallophores.

10 The mechanisms of staphylopin biosynthesis export and recovery of the metal
11 complexes are summarized in Fig. 4. The biosynthesis of staphylopin aggregates three
12 unprecedented enzyme activities with the use of D-histidine, the fusion of a single α -
13 aminobutyric acid moiety from SAM, and the fabrication of an opine derivative. This latter
14 activity was so far restricted to plant's bacterial transfection or anaerobic glycolysis in marine
15 invertebrates (19, 23). The use of histidine as a building block is interesting as the free amino
16 acid has a relatively high affinity for nickel on its own and is directly used for nickel uptake by
17 bacteria (8, 24-26). However, the use of the D- stereoisomer of histidine is surprising because D-
18 amino acids are mainly used in cell wall biosynthesis and have been mostly restricted to alanine
19 and glutamate (27), although other "non-canonical" D-amino acids are reported to be involved in
20 the composition of the cell wall (28, 29), in biofilm stability (30), virulence (31) or sporulation
21 (32). Another peculiarity of the staphylopin biosynthetic machinery resides in the NAS-like
22 CntL enzyme that only uses one α -aminobutyric acid moiety from SAM, whereas the NAS-like
23 from *M. thermotautrophicum* uses two, and plant enzymes use three such moieties. Interestingly,
24 the evolution from bacterial staphylopin to plant's nicotianamine preserves a large part of the
25 molecule's backbone, therefore suggesting a conservative chemical evolution going together
26 with enzymatic simplifications wherein plant nicotianamine is synthesized by a single enzyme.
27 Finally, homologous genes involved in staphylopin biosynthesis are conserved in other
28 pathogenic bacteria such as *Yersinia pestis* or *Pseudomonas aeruginosa* underscoring the likely
29 influence of this metallophore in bacterial pathogenicity. Indeed, the export pathway of this
30 metallophore was recently identified as a critical function for the growth of *P. aeruginosa* in
31 airway mucus secretions where metal access is severely limited (33).

32
33

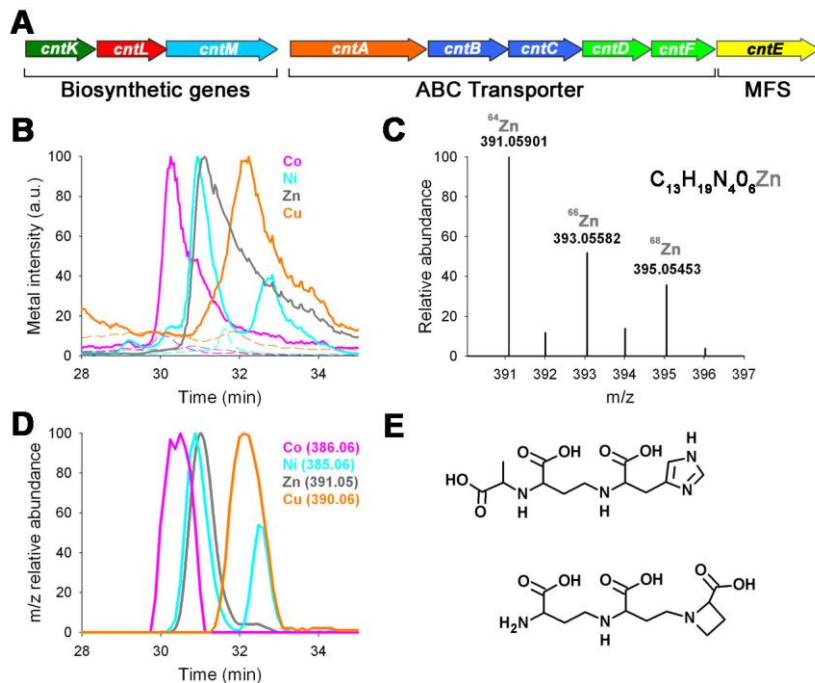
1 References and Notes:

- 2 1. M. L. Reniere, G. Pishchany, E. P. Skaar, in *Iron uptake and homeostasis in*
3 *microorganisms*. (2010).
- 4 2. B. D. Corbin *et al.*, *Science* **319**, 962 (2008).
- 5 3. M. I. Hood, E. P. Skaar, *Nat Rev Microbiol* **10**, 525 (2012).
- 6 4. Z. Ma, F. E. Jacobsen, D. P. Giedroc, *Chem Rev* **109**, 4644 (2009).
- 7 5. A. G. Bobrov *et al.*, *Mol Microbiol* **93**, 759 (2014).
- 8 6. I. J. Schalk, M. Hannauer, A. Braud, *Environ Microbiol* **13**, 2844 (2011).
- 9 7. H. J. Kim *et al.*, *Science* **305**, 1612 (2004).
- 10 8. H. Lebrette *et al.*, *Metallomics* **7**, 613 (2015).
- 11 9. K. Schauer, B. Gouget, M. Carriere, A. Labigne, H. de Reuse, *Mol Microbiol* **63**, 1054
12 (2007).
- 13 10. L. Remy *et al.*, *Mol Microbiol* **87**, 730 (2013).
- 14 11. C. Curie *et al.*, *Ann Bot* **103**, 1 (2009).
- 15 12. E. L. Walker, B. M. Waters, *Curr Opin Plant Biol* **14**, 318 (2011).
- 16 13. R. Hell, U. W. Stephan, *Planta* **216**, 541 (2003).
- 17 14. A. Herbig *et al.*, *Eur J Biochem* **265**, 231 (1999).
- 18 15. K. Higuchi *et al.*, *Plant Physiol* **119**, 471 (1999).
- 19 16. H. Q. Ling, G. Koch, H. Baumlein, M. W. Ganai, *Proc Natl Acad Sci U S A* **96**, 7098
20 (1999).
- 21 17. C. Dreyfus, D. Lemaire, S. Mari, D. Pignol, P. Arnoux, *Proc Natl Acad Sci U S A* **106**,
22 16180 (2009).
- 23 18. S. H. Smits, A. Mueller, L. Schmitt, M. K. Grieshaber, *J Mol Biol* **381**, 200 (2008).
- 24 19. M. Harcet, D. Perina, B. Plese, *Biochem Genet* **51**, 666 (2013).
- 25 20. M. W. Bevan, M. D. Chilton, *Annu Rev Genet* **16**, 357 (1982).
- 26 21. Y. Ding, Y. Fu, J. C. Lee, D. C. Hooper, *J Bacteriol* **194**, 6586 (2012).
- 27 22. Materials and methods available on Science online.
- 28 23. J. Thompson, J. A. Donkersloot, *Annu Rev Biochem* **61**, 517 (1992).
- 29 24. P. T. Chivers, E. L. Benanti, V. Heil-Chapdelaine, J. S. Iwig, J. L. Rowe, *Metallomics* **4**,
30 1043 (2012).
- 31 25. H. Lebrette, M. Iannello, J. C. Fontecilla-Camps, C. Cavazza, *J Inorg Biochem* **121**, 16
32 (2013).
- 33 26. M. M. Shaik, L. Cendron, M. Salamina, M. Ruzzene, G. Zanotti, *Mol Microbiol* **91**, 724
34 (2014).
- 35 27. W. Vollmer, D. Blanot, M. A. de Pedro, *FEMS Microbiol Rev* **32**, 149 (2008).
- 36 28. F. Cava, M. A. de Pedro, H. Lam, B. M. Davis, M. K. Waldor, *Embo J* **30**, 3442 (2011).
- 37 29. H. Lam *et al.*, *Science* **325**, 1552 (2009).
- 38 30. I. Kolodkin-Gal *et al.*, *Science* **328**, 627 (2010).
- 39 31. A. T. Anfora, B. J. Haugen, P. Roesch, P. Redford, R. A. Welch, *Infect Immun* **75**, 5298
40 (2007).
- 41 32. K. A. O'Connor, D. R. Zusman, *Mol Microbiol* **24**, 839 (1997).
- 42 33. M. Gi *et al.*, *Sci Rep* **5**, 14644 (2015).

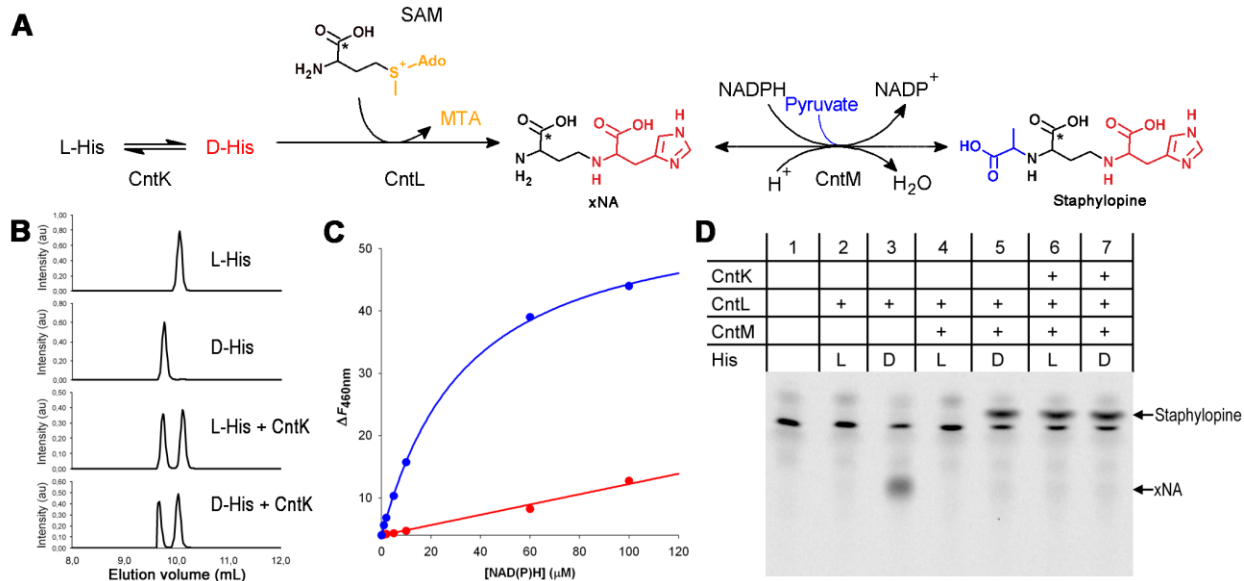
43
44
45
46

1 **Acknowledgments:** We thank the Commissariat à l’Energie Atomique et aux Energies
2 Alternatives (CEA), the Agence Nationale de la Recherche (ANR) and the CEA program
3 ToxNuc-E for financial support. Support was also provided by the HélioBiotec platform (funded
4 by the European Regional Development Fund, the Région Provence Alpes Côte d’Azur, the
5 French Ministry of Research, and the “Commissariat à l’Energie Atomique et aux Energies
6 Alternatives”). G. G. was supported by the Région PACA. Work at the F. C. lab was supported
7 by MIMS, KAW, the Swedish Research Council and a Kempe foundation scholarship to A. E.
8 We wish to thank J. Lavergne for careful reading of the manuscript and we also thank A.
9 Verméglio, C. Cavazza and H. Lebrette for fruitful discussions.
10

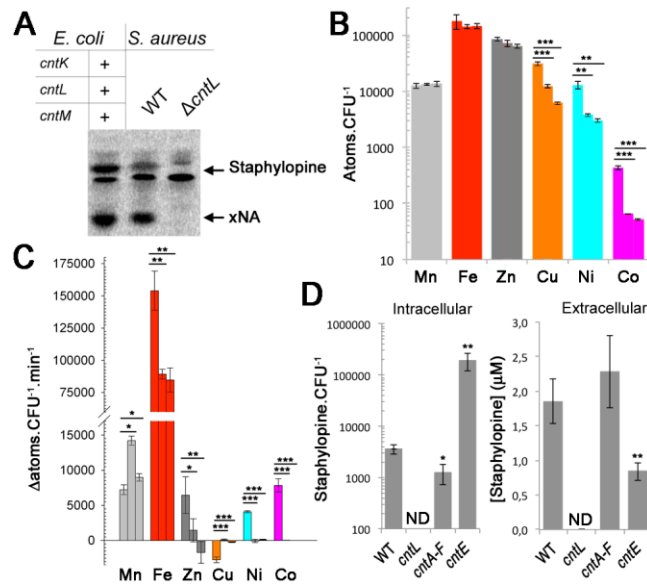
1 **Figure and Figure Legends**



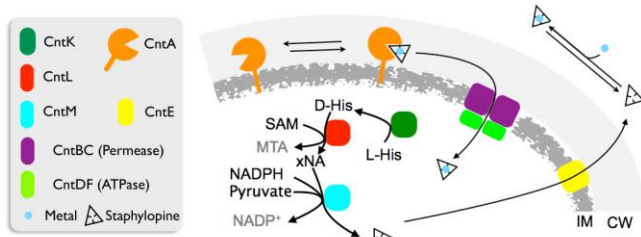
2
 3 **Fig. 1. The *cnt* operon and detection of a broad-spectrum metallophore.** (A) The *cnt* operon
 4 encodes three putative biosynthetic genes together with the genes coding for a full ABC
 5 transporter and a transporter belonging to the MFS family. (B) HILIC/ICP-MS chromatograms
 6 of extracellular fractions of *S. aureus* and comparison of the WT strain (plain line) with the *cntL*
 7 mutant (dotted lines). (C) Mass spectra of a chelating compound present in its free and
 8 complexed forms (here shown in complex with Zn) in the extracellular fraction of the WT strain
 9 but absent in the *cntL* mutant as observed in chromatogram around 31 min during HILIC/ESI-
 10 MS analyses. The empirical molecular formula was deduced from exact masses. (D) HILIC/ESI-
 11 MS extracted ion chromatograms (XIC) of some metal-ions observed to form a complex with the
 12 above-mentioned chelator. Chromatograms were traced using the exact masses (± 3 ppm) of the
 13 expected complex and these masses were absent in the extracellular fraction of the *cntL* mutant.
 14 (E) Proposed chemical structure of staphylopin (top) and comparison with nicotianamine
 15 (bottom).
 16



1
 2 **Fig. 2. Biosynthesis of staphylopine and biochemical characterization of the biosynthetic**
 3 **enzymes.** (A) Biosynthesis pathway for the assembly of staphylopine from L-histidine, SAM and
 4 pyruvate. (B) Epimerase assay of CntK and comparison with L- and D-histidine standards. (C)
 5 Titration of NADH (red) and NADPH (blue) binding to CntM (5 μ M) followed by fluorescence
 6 energy transfer between tryptophan excitation (280 nm) and NAD(P)H emission (460 nm).
 7 Fitting of the data obtained for NADPH binding lead to a K_d of 50 μ M. (D) TLC separation of
 8 reaction products incubating [14 C]-SAM (labeled on its α -aminobutyric acid moiety; marked
 9 with a * in panel A) with various purified enzymes, pyruvate, NADPH and either L- or D-
 10 Histidine.
 11



1
 2 **Fig. 3. Effect of *cnt* mutations in metal content and staphylopine localization.** (A) TLC
 3 separation of co-incubation of *E. coli* cell extracts separately expressing CntK, CntL and CntM
 4 with [¹⁴C]-SAM and comparison with the cell extracts from WT *S. aureus* and *cntL* mutant
 5 strains. (B) Intracellular metal content of the *S. aureus* WT (left), *cntL* (middle) and *cntA-F*
 6 (right) strains grown in CDM, and determined by ICP-MS. Error bars, mean ± s.d. ***P*<0.01 and
 7 ****P*<0.001. (C) Intracellular metal content change of the *S. aureus* WT (left), *cntL* (middle) and
 8 *cntA-F* (right) strains grown in dCDM until late exponential phase (T₀) and then incubated 10
 9 minutes with 0.3μM Fe(II), Zn, and 0.1μM Mn, Ni, Co, Cu. Metal content variation was
 10 determined by ICP-MS and expressed as the differential of atoms after 10 min. as compared to
 11 T₀. Error bars, mean ± s.d. **P*<0.05, ***P*<0.01 and ****P*<0.001. (D) Staphylopine level in the
 12 intracellular (left; note the logarithm scale) and supernatant (right) fractions of the WT,
 13 *cntABCDF*, *cntL* and *cntE* mutant strains. Error bars, mean ± s.d. **P*<0.05 and ***P*<0.01, ND:
 14 Not detected.
 15



1
 2 **Figure 4: Model of staphylopine biosynthesis, export and recovery of staphylopine-metal**
 3 **complexes through the ABC transporter. IM: Inner Membrane, CW: Cell Wall.**

1 **Supplementary Materials**

2 Materials and Methods

3 Figs. S1-S16

4 Tables S1-S3

5 Refs (34-49)

6

1 **Supplementary Materials:**

2 **Materials and Methods**

3 *Bioinformatic analysis*

4 Sequences from CntK (encoded by *sav2470*), CntL (*sav2469*) and CntM (*sav2468*) were
5 analyzed by searching for homologues using PsiBLAST (34) and the Pfam database (35).
6 Sequence alignment was done using the Muscle program (36) and visualized in the Jalview suite
7 (37). The threading program Phyre2 (38) was used to detect distant homologues. Gene synteny
8 were inspected using the MaGe MicroScope web interface (39).

9

10 *Gene cloning, protein expression and purification*

11 The entire operon from *S. aureus* (9,3 kb; from *cntK* to *cntE*; *sav2470* to *sav2462*) was amplified
12 by PCR (See Table S1 for oligonucleotides used in this study). The resulting fragment was
13 digested by NdeI and XhoI and ligated in plasmid pET22b+. The three biosynthetic genes (*cntK*,
14 *cntL* and *cntM*) and the *cntA* gene were separately cloned in pET100, pET-SUMO, pET101 and
15 pET100, respectively, according to standard protocols. After co-transformation with plasmid
16 pRARE (encoding for rare codon in *E. coli* BL21) strains were cultivated in LB media
17 supplemented with appropriate antibiotics. When the OD of the culture was about 0.6 they were
18 transferred at 16 °C and protein expression was induced by adding 0.1 mM IPTG. Bacteria were
19 recovered after overnight growth by centrifugation at 7,000 g for 15 min. Cells were resuspended
20 in buffer A (20 mM Na,K PO₄ (pH 7.5), 500 mM NaCl, 20 mM imidazole) and disrupted using a
21 French press operating at 1000 psi. Cell debris were removed by centrifugation at 8,000 g for 20
22 min. The supernatant was centrifuged at 100,000 g for 1 h at 4°C to remove cell wall debris and
23 membrane proteins. The resulting soluble fraction was loaded on a nickel affinity column
24 (HisTrap 1 ml column, G.E. Healthcare), and the protein was eluted stepwise with imidazole (75
25 mM wash and 250 mM elution). Collected fractions were loaded onto a gel filtration column
26 (Hiload 26/60 Superdex 200, G.E. Healthcare), equilibrated with buffer B (20 mM HEPES, 50
27 mM NaCl pH 8.0) for CntA, CntK and CntL, or buffer C (buffer B + 500 mM NaCl) for CntM.
28 Before gel filtration, the tag of CntL was removed by incubating the protein (1 mg/mL) with the
29 SUMO (Ulp-1) protease using a protein / protease ratio of 1/100 (w/w) and an overnight
30 incubation at room temperature. Protease, free tag and uncleaved protein were then removed by a
31 second passage through a Ni-NTA column equilibrated with buffer A.

32

33 *Construction of cntL and cntE deletion mutants of S. aureus and complementation*

34 A deletion mutant of *S. aureus* RN6390 was obtained as described (40). Briefly, two DNA
35 fragments corresponding to upstream and downstream regions of *cntL* or *cntE* gene were
36 amplified from RN6390 chromosomal DNA using primers pairs listed in Table S1. Deletion
37 fragments were generated using splicing by overlap extension PCR and cloned into BamHI (for
38 *cntL* mutant) or BamHI and XmaI (for *cntE* mutant) sites of shuttle vector pMAD (41). The
39 resulting plasmid was introduced into *S. aureus* RN4220 by electroporation, extracted and
40 subsequently introduced into *S. aureus* RN6390. Deletion of the chromosomal region of interest
41 was subsequently obtained by double-crossing over events as previously described (42). To
42 complement the *cntL* deletion strain, the *cntL* gene was amplified by PCR (Table S1) and

1 inserted into BamHI site of shuttle vector pOS1-*Plgt* to generate pCntL in which *cntL* is under
2 the control of the *lgt* promoter (43). Recombinant vectors (pOS1-*Plgt* and pCntL) were
3 introduced into *S. aureus* strains as described above.

4
5 *Cell culture conditions* WT and mutant strains of *S. aureus* were grown at 37°C with aeration in
6 either CDM (40, 44) deprived of added metals except magnesium (1 mM; Table S2),
7 demetalated CDM (CDM treated with chelex; dCDM) or LB. For cultures in CDM with metal-
8 NTA resin (rCDM), NTA-treated CDM and metalated resin were prepared as follows: Ni-NTA
9 His-bind resin (EMD Millipore, Billerica) was extensively washed with 100mM EDTA (~15
10 time the resin volume) to eliminate nickel linked to NTA, and then with double distilled water to
11 remove EDTA. CDM was then incubated overnight with the demetalated NTA resin and further
12 filtrated to obtain NTA-treated CDM. The resin (now metalated by the traces of metals present in
13 CDM) was then placed into Amicon centrifugal filter units (Amicon Ultra-0.5ml 3KDa; Merck
14 Millipore, Tullagreen) inserted into eppendorf tubes. After having cut the bottom of these tubes,
15 they were introduced into 50 ml Falcon tubes containing the NTA-treated CDM. Despite
16 demetalation by EDTA, the total amounts of metal in rCDM treated cells seems to indicate that
17 residual amounts of Mn, Cu and Ni remained trapped by the resin as the uptake of these metals
18 was found higher in rMCD cells than CDM cells. For short time uptake experiments, strains
19 were grown in demetalated CDM until late exponential phase, then supplemented with a metal
20 cocktail (0.3µM Fe(II) and Zn; 0.1µM Ni, Co, Cu, Mn) and incubated for 10 minutes prior to
21 metal level determination by ICP-MS.

22 23 *Analysis of metal concentrations by ICP-MS*

24 Metal content of the media used in this study are reported in Table S3. After growing until late
25 exponential phase or overnight, the cultures (15 mL) were centrifuged and pellets were washed
26 three times with ice cold 1mM EDTA and then once with double distilled water. Cells were then
27 dried overnight at 100 °C. Metal contents were determined in cell fraction by resuspending the
28 dried pellet with a 200 µL mixture of 70% HNO₃ (100 µL) and 30% H₂O₂ (100 µL). The mixture
29 was heated at 80°C for 3 h and then diluted with water to reach a final volume of 2 mL.
30 Acidified sample solutions were then analyzed by ICP-MS (Agilent 7500cs) operating in
31 hydrogen collision gas mode (H₂) to remove possible interferences.

32 33 *Cell fractionation for staphylopine quantification and TLC assay*

34 WT and mutant strains of *S. aureus* were grown in CDM at 37°C with aeration, centrifuged, and
35 the supernatants were collected, filtrated and stored at -20°C. The pellets were resuspended in 2
36 ml lysis buffer (0.1 mg /ml lysostaphin in Hepes 20 mM) and incubated at 37°C for 1 h by
37 shaking (150 rpm). Lysates were then transferred into tubes containing 0.1 mm glass beads (MP
38 Biomedicals, Solon, OH) and subjected to mechanical disruption by homogenization using a
39 FastPrep FP120 instrument (Thermo Scientific, Waltham) in three 45 s intervals at a speed of
40 6.0, with cooling on ice between intervals. The lysates were centrifuged at 14,000 g for 20 min at
41 4°C and supernatants were collected. Staphylopine level determination is described further
42 below.

1 *Analysis of metal complexes using HILIC/ICP-MS*

2 This separation method preserves metal-ligand complexes and facilitates their downstream
3 identification (45, 46). Analytical reagent grade chemicals such as acetonitrile, acetic acid,
4 formic acid, nitric acid and ammonia were purchased from Sigma-Aldrich (Saint-Quentin-
5 Fallavier, France). Ultrapure water (18 M Ω .cm) was obtained from a Milli-Q system (Millipore,
6 Bedford, MA). Microbore HILIC separations were performed using an Agilent 1100 capillary
7 HPLC system (Agilent, Tokyo, Japan) equipped with a 100 μ l min⁻¹ splitter module. ICP-MS
8 detection was achieved using a model 7500cs instrument (Agilent) fitted with platinum cones, 1
9 mm i.d. injector torch and a T-connector allowing the introduction of 5% O₂. The HILIC/ICP-
10 MS coupling was done via an Isomist interface (Glass Expansion, Melbourne, Vic, Australia)
11 consisting of a 20-ml Cinnabar cyclonic spray chamber cooled to 2 °C and fitted with a 50 μ l
12 min⁻¹ Micromist U-series nebulizer.

13 The column used for HILIC separation was a TSK gel amide 80 (250 mm \times 1 mm i.d., 5 μ m)
14 from Tosoh Biosciences (Stuttgart, Germany). Gradient elution, at a flow rate of 50 μ l min⁻¹, was
15 carried out using eluent A, acetonitrile, and eluent B, 5 mM ammonium formate (pH 5.5). The
16 gradient program was: 0–5 min 10% B, 5–45 min up to 50% B, 45–50 min 50% B, 50–52 min up
17 to 65% B, 52–55 min 65% B, 55–60 min down to 10% B, 60–65 min 10% B. Samples were
18 diluted with acetonitrile and water to obtain a 1 : 2, sample to acetonitrile ratio, and centrifuged.
19 A 7- μ l aliquot of the supernatant was injected into the HILIC column each time.

20

21 *Analysis for metal complexes using HILIC/ESI-MS*

22 For HILIC/ESI-MS, the HPLC systems were connected to an LTQ Orbitrap Velos mass
23 spectrometer (Thermo Fisher Scientific, Bremen, Germany). The coupling was achieved via a
24 heated electrospray ionization source (H-ESI II) (Thermo Fisher Scientific. The ion source was
25 operated either in the positive ion mode at 3.0 kV. The vaporizer temperature of the source was
26 set to 120 °C and the capillary temperature to 280 °C. In full MS mode, the resolution was set at
27 100 000 (FWHM at m/z 400) whereas in MS/MS mode it was set at 30 000. MS data were
28 processed using Xcalibur 2.1 software and MetWorks 1.2.1 software (Thermo Fischer Scientific)
29 to screen spectra for metal containing molecules. To get accurate masses, MS and MS/MS
30 spectra were recalibrated offline using precursor/fragment ions with known formula. Putative
31 metal species were fragmented during a subsequent chromatographic run with collision induced
32 dissociation (CID) mode at 35% energy. In order to fit the molecular formula that we obtained
33 from accurate masses, we used simple chemical rules as follow: 1/ each time there is a reductive
34 condensation there is a mass loss of 16 Da between the two reactants. 2/ each time there is an α -
35 aminobutyric acid moiety transfer from SAM to an amino acid there is a mass loss of 2 Da
36 between the two reactants. This way, the “simplest” molecule would consist of pyruvate (88Da)
37 reductively condensed with glycine (75 Da) that would be modified by two α -aminobutyric
38 acid moieties (103 Da), which would give a molecular weight of 349 Da, above the 328 Da
39 measured. The only possibility is therefore to use only one α -aminobutyric acid moiety from
40 SAM; and only using histidine (155 Da) and pyruvate we can obtain the expected 328 Da.

41

42 *Determination of metal binding affinity and quantification of synthetic staphylopine*

1 Synthetic staphylopin (N-[3-(N-L-Alanyl)-amino-3-carboxypropyl]-D-histidine) was ordered to
2 Toronto Research Chemical Inc (Toronto, Canada) and its NMR spectrum is provided in Fig.
3 S16. Metal content of the studied elements in staphylopin synthetic standard was measured by
4 ICP MS and was found to be lower than 0.1% of staphylopin mass. Analysis of this synthetic
5 standard by HILIC/ESI-MS showed that it has the same retention time, chromatographic peak
6 shapes, fragmentation behavior in MS instrument and metal affinity than the natural molecule
7 found in culture supernatants. It was then used also to quantify staphylopin in spent culture
8 media through standard addition technique, which resulted in staphylopin peak increases during
9 HILIC/ESI-MS analysis and which allow to determine staphylopin concentration and confirmed
10 results obtained by HILIC/ICP-MS analysis. We tested metal affinity of staphylopin standard
11 by mixing different metals (Fe(II), Fe(III), Cu, Zn, Co, Ni) with this molecule prior to direct
12 analysis by ESI-MS. It was found that metal affinity for staphylopin was in the following order:
13 Cu(II) > Ni > Co > Zn > Fe(II) > Mn(II), which is identical to what was observed for
14 nicotianamine. Fe(III) affinity for staphylopin relative to other metals is pH dependent and,
15 whereas it has a higher pKd value than Cu(II), Fe(III) has a poor affinity for staphylopin at
16 neutral pH, a phenomenon already described for nicotianamine (47). Stability constants for
17 staphylopin:metal complexes were estimated by metal competition experiments with
18 nicotianamine. Mixtures of nicotianamine:staphylopin:metal were analyzed in physiological
19 conditions (pH = 7) by infusion in ESI MS. Were analyzed: 1) a mixture of only nicotianamine
20 and staphylopin at 100µM each to establish maximal signal intensity for these free ligands, 2) a
21 mixture of nicotianamine (100 µM), staphylopin (100µM) and an excess of metal (1mM, each
22 metal was tested in a different experience) to establish maximal signal intensity for the
23 complexed ligands and 3) a mixture of nicotianamine (100 µM), staphylopin (100µM) and
24 limited level of metal (80µM, each metal was tested in a different experience) to created
25 competition and observed the proportion between metal complexes formed. The estimated pKd
26 values are given in Fig. S15C. Like nicotianamine also, the complex of staphylopin with metal
27 is only observed as a 1:1 complex during ESI MS analysis. All these data lead to consider that
28 staphylopin is very similar to nicotianamine in terms of metal affinity and structure. A putative
29 model for metal:staphylopin complex can then be proposed (hexadentate structure with 3 amino
30 groups (the ones spaced by 3 carbons) and the 3 carboxylic groups, Fig. S15A).

31

32 *Fishing and Metabolomic studies*

33 The CntA protein, predicted to bind the metallophore-nickel complex, was purified by
34 conventional HisTrap and incubated in 50 mL of a culture supernatant from a *cntA* mutant of *S.*
35 *aureus* cultivated in CDM. Nickel was then added to a final concentration of 50 µM to allow the
36 nickel-metallophore complex to form and to bind to CntA. After 2 h of incubation the CntA
37 protein was purified again, exchanged against a buffer containing 10 mM ammonium acetate,
38 and finally analyzed by MS. Cell fraction of an *E. coli* strain expressing the entire *cnt* operon
39 was also analyzed by HILIC/ICP-MS for metal detection and HILIC/ESI-MS for metabolite and
40 metal complex identification.

41

42 *Metal content using ICP-AES (atomic emission spectroscopy)*

43 *S. aureus* strains were grown at 37 °C with aeration in LB medium or in CDM until late
44 exponential phase. In CDM condition, nickel, copper, zinc or cobalt chloride was then added (1

1 μM final). Cultures were then grown overnight and harvested by centrifugation at 6,000 g at 4°C
2 for 15 min. Pellets were washed three times with ice-cold 1 mM EDTA and once in double
3 distilled water. Cells were dried overnight at 100°C and then digested with 500 μl of nitric acid
4 (70 % HNO_3 ICP Grade, JT Baker) overnight at 80°C. Samples were further diluted by addition
5 of distilled water (final volume 6 mL). The element measurements were performed with
6 Inductively Coupled Plasma – Absorption Emission Spectrometer (ICP-AES Vista MPX,
7 Varian). The metal concentrations were determined using standard curves obtained by analyzing
8 ICP grade element standard solutions. The metal contents were calculated assuming 4×10^8
9 CFU (Colony Forming Unit) for an OD600 of 1 unit, as determined by plating diluted cultures
10 grown in CD medium.

11

12 *Fluorescence studies and microcalorimetry*

13 Fluorescence studies were performed using a Cary Eclipse spectrophotometer (Agilent). The
14 FRET experiment was done using a protein concentration of 5 μM an excitation wavelength at
15 280 nm. The signal was recorded between 400 and 500 nm. Five spectra were averaged in order
16 to increase signal to noise ratio. The dissociation constants were obtained by directly fitting the
17 experimental data to a binding equation in SigmaPlot.

18 Microcalorimetry was used to determine the dissociation constants for the binding of NADPH to
19 CntM using a MicroCal iTC200 system (MicroCal). The experiments were performed at 25 °C in
20 buffer C. Titration experiments consisted of 13 injections (3 μL) of NADPH (1 mM in buffer C)
21 to 200 μL of protein (97 μM). Dissociation constant was obtained using one set of sites fitting in
22 Origin (MicroCal).

23

24 *Epimerase/Racemase assay*

25 The product from a racemization reaction (30 μg of purified CntK incubated during 30 min at
26 room temperature in 100 mL of buffer (Na,K phosphate 50 mM pH 8.0, DTT 1 mM) and
27 supplemented with 20 mM L- or D-amino acids) was derivatized with L-FDAA (1-fluoro-2-4-
28 dinitrophenyl-5-L-alanine amide, Marfey's reagent, Thermo Scientific). First, an equal volume
29 of NaHCO_3 0.5 M was added to the racemization reaction; then, 6 μl of this reaction were
30 reacted with L-FDAA (10 mg/mL in acetone) at 80°C for 3 min. The reaction was stopped with 2
31 N HCl and the samples were filtered. The products were separated at 2 mL/min with a linear
32 gradient of triethylamine phosphate/acetonitrile in HPLC for 45 min with an Aeris peptide
33 column (250 x 4.6 mm; 3.6 μm particle size) (Phenomenex, USA) and detected at 340 nm. For
34 the co-incubation with alanine or methionine, the flow was 1 mL/min and the gradient length
35 was set to 105 min. Background noise was removed from the L,D-His racemization reactions
36 graphics.

37

38 *Activity assay followed by TLC*

39 Cellular fractions of *S. aureus* WT and *cntL* mutant strains were supplemented with EDTA and
40 DTT (1 mM final) prior to the TLC assay. [^{14}C]-SAM (BioTrend, Köln, Germany) was added to
41 the cell fraction(s) at a final concentration of 20 μM , together with 1mM pyruvate and 100 μM
42 NADPH in order to ensure that there was enough substrate during the assay. The assay using

1 purified proteins consisted in incubating the enzymes, either separately or by co-incubation, at a
2 final concentration of 3 μM and using [^{14}C]-SAM (20 μM), NAD(P)H (30 μM), L- or D-histidine
3 (10 μM) and α -keto acid (pyruvate or α -keto glutarate; 1mM). The total volume was 100 μL in
4 buffer D (HEPES 50 mM, DTT 1 mM, EDTA 1 mM, pH 9.0). The mixture was incubated for 30
5 min at 28 $^{\circ}\text{C}$. The reactions were stopped by adding ethanol to a final concentration of 50 % (v/v)
6 and the products were then separated by TLC. An aliquot of 10 μL of the reaction mixtures were
7 spotted on HPTLC (High Performance TLC) Silica Gel 60 Glass Plates (Merck KGaA), and the
8 plates were developed with a phenol:*n*-butanol:formate:water (12:3:2:3 vol/vol) solvent system.
9 These separation parameters were used in the initial biochemical characterization of plant
10 nicotianamine synthase (48). HPTLC plates were dried and exposed to a [^{14}C]-sensitive imaging
11 plate for 2-3 days. Imaging plates were then scanned on a Typhoon FLA 7000 phosphorimager
12 (GE Healthcare).

13

14 *Construction of promoter-reporter gene fusion and luciferase assays.*

15 The reporter gene *luxAB* from *Vibrio fischeri* cloned into shuttle vector pCN58 was used for gene
16 expression analysis. The *cntK* upstream region (569bp) was cloned using oligonucleotides
17 indicated in Table S1, as previously described for the *cntA* promoter (10). To follow the *cnt*
18 promoter-luciferase reporter activity, CDM and LB media were inoculated with an overnight
19 culture to obtain an optical density (OD_{600}) of 0.1 or 0.05, respectively. Culture aliquots were
20 removed, monitored for growth (OD_{600}), and submitted to luminescence assays. Measurements
21 of luminescence were performed immediately after mixing 450 μl of cell suspension with 50 μl
22 of 0.1 % (vol/vol in 40 % ethanol) nonanal (Sigma, St Louis, MO). Luciferase activity, expressed
23 in relative luminescence units (RLUs), was measured using a Biolumat LB9500T Luminometer
24 (Berthold, Bad Wildbad, Germany), based on 10 s measurements in the integrate data mode.
25 Specific luciferase activities were calculated by dividing the RLUs by absorbance ($\text{RLU}/\text{OD}_{600}$).
26 The promoterless pCN58 plasmid was used as control in reporter gene assays.

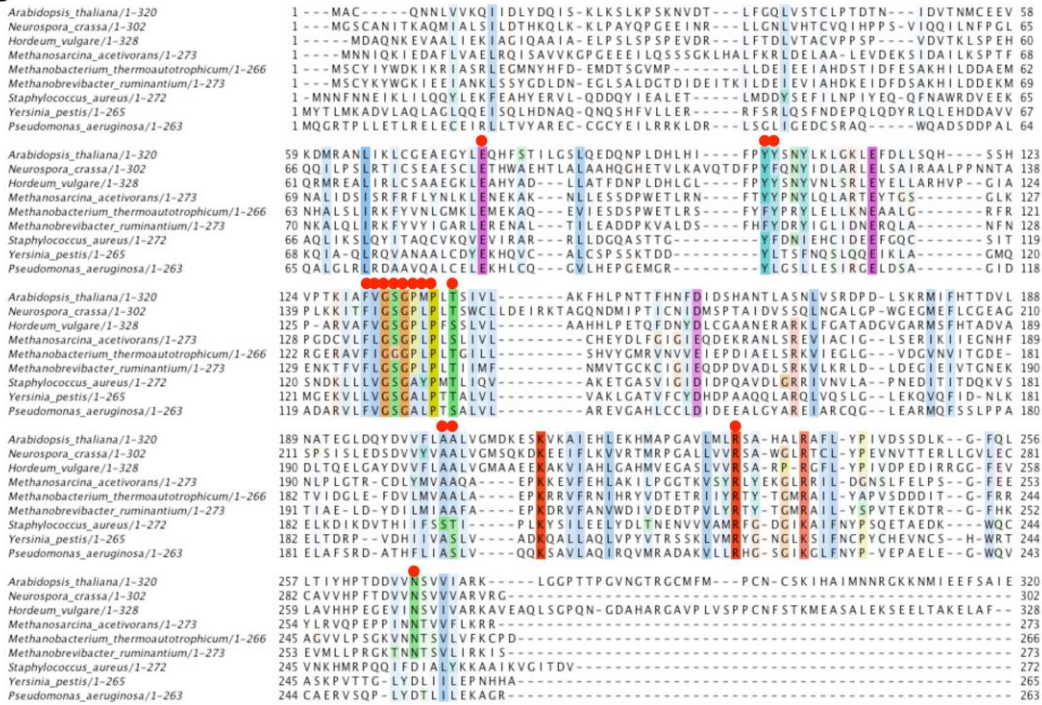
27

1 Supplementary Figures and Table

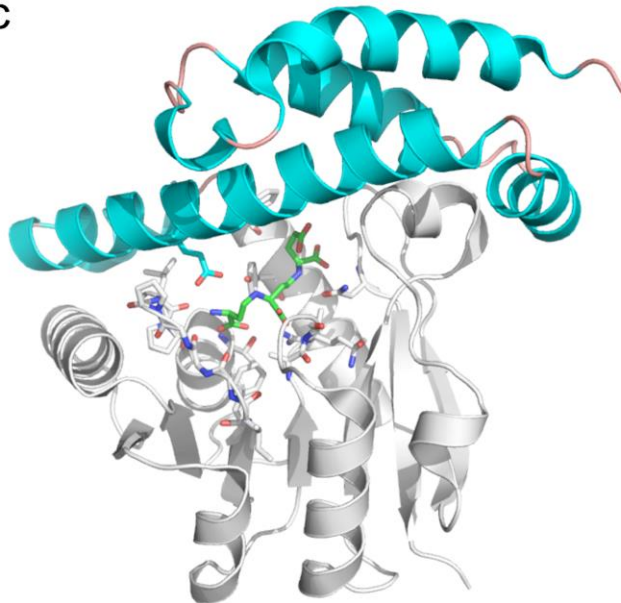
A

Protein	Blast	Pfam	Threading
CntK	DapF (Diaminopimelate epimerase)	-	DapF (100%)
CntL	Alcohol dehydrogenases of the MDR family	FmrO (Ribosomal Methyltransferase)	NAS/NAS-like (100%)
CntM	DUF2338	DUF2338	Octopine dehydrogenase (100%)

B



C



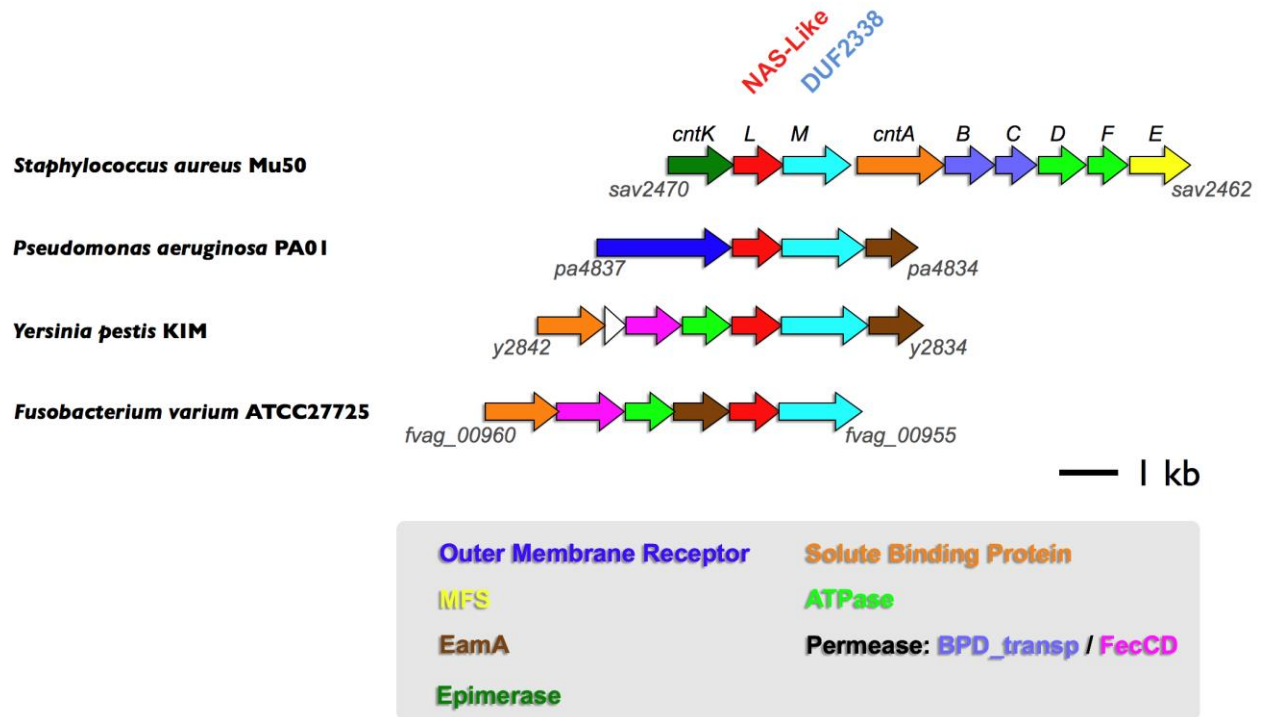
2

3 **Figure S1: Sequence analysis of the three putative enzymes located in the *cnt* operon. (A)**
 4 **Summary of sequence analysis of CntK, CntL and CntM protein sequences through PSI-Blast,**
 5 **Pfam and Phyre2. (B) Sequence alignment of three eukaryotic NAS, three archaeal NAS-Like**

1 and three bacterial NAS-Like enzymes, including CntL from *S. aureus*. Threshold for the
2 ClustalX coloring scheme correspond to 30 % sequence conservation as defined in Jalview.
3 Residues marked by a red dot are conserved residues that are located near the
4 thermonicotianamine (tNA) product in the structure of an archaeal NAS-Like enzyme shown in
5 C. (C) Structure of an archaeal NAS-Like enzyme (pdb code 3FPE) in complex with its product
6 tNA (represented in green stick). The N-Terminal domain is colored in blue (helices) and salmon
7 (loops), and the C-Terminal domain in light gray. Side chains of conserved residues in the
8 sequence alignment (labeled with a red dot in B) are represented in stick. Most of the conserved
9 residues are located closed to the tNA product, therefore clearly indicating that bacterial NAS-
10 like enzymes are related to the NAS family.

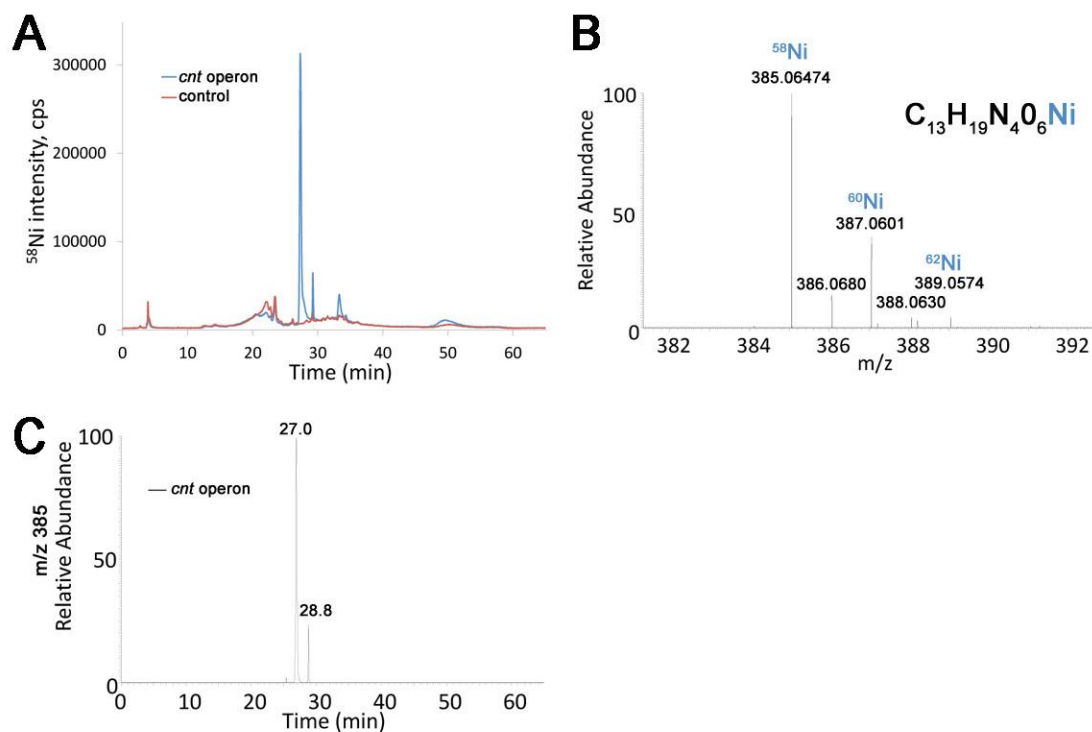
11

1



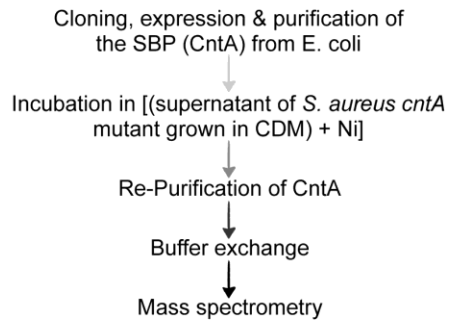
2

3 **Figure S2: Synteny of the NAS-like encoding gene in selected bacteria.** Genes are color-
4 coded as a function of the Pfam family to which the product belongs, as indicated in the grey
5 inset. *Y. pestis*, *P. aeruginosa* and *F. varium* does not possess a close CntK homologue but a
6 distantly related protein that is annotated as diaminopymelate epimerase (DapF).
7

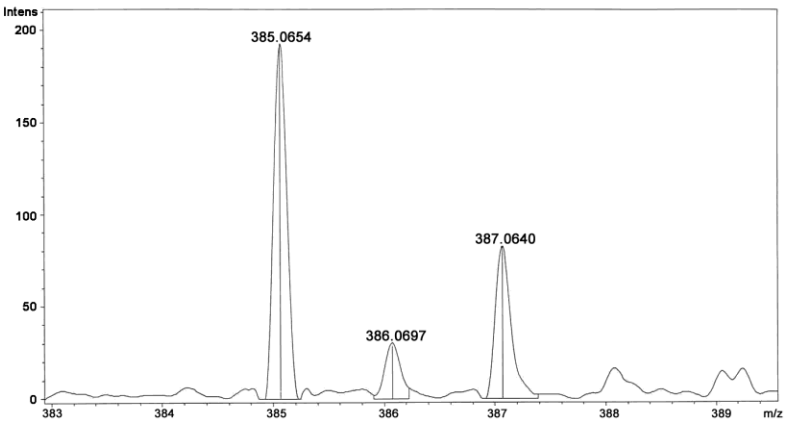


1
2 **Figure S3: Metabolomic study of *E. coli* strains expressing the *cnt* operon or the empty**
3 **vector.** (A) HILIC/ICP-MS chromatograms of intracellular fractions of *E. coli* strain
4 (supplement with 0.1 μ M nickel to ensure a nickel complexation of the metallophore) and
5 expressing the *cnt* operon from *S. aureus* (blue line) and comparison with the strain expressing
6 the empty vector (red line). (B) Mass spectra of a chelating compound present in its complexed
7 forms with nickel. Molecular formula was deduced from the exact mass of the ^{58}Ni complex. (C)
8 HILIC/ESI-MS extracted ion chromatograms of m/z 385.06.
9

A

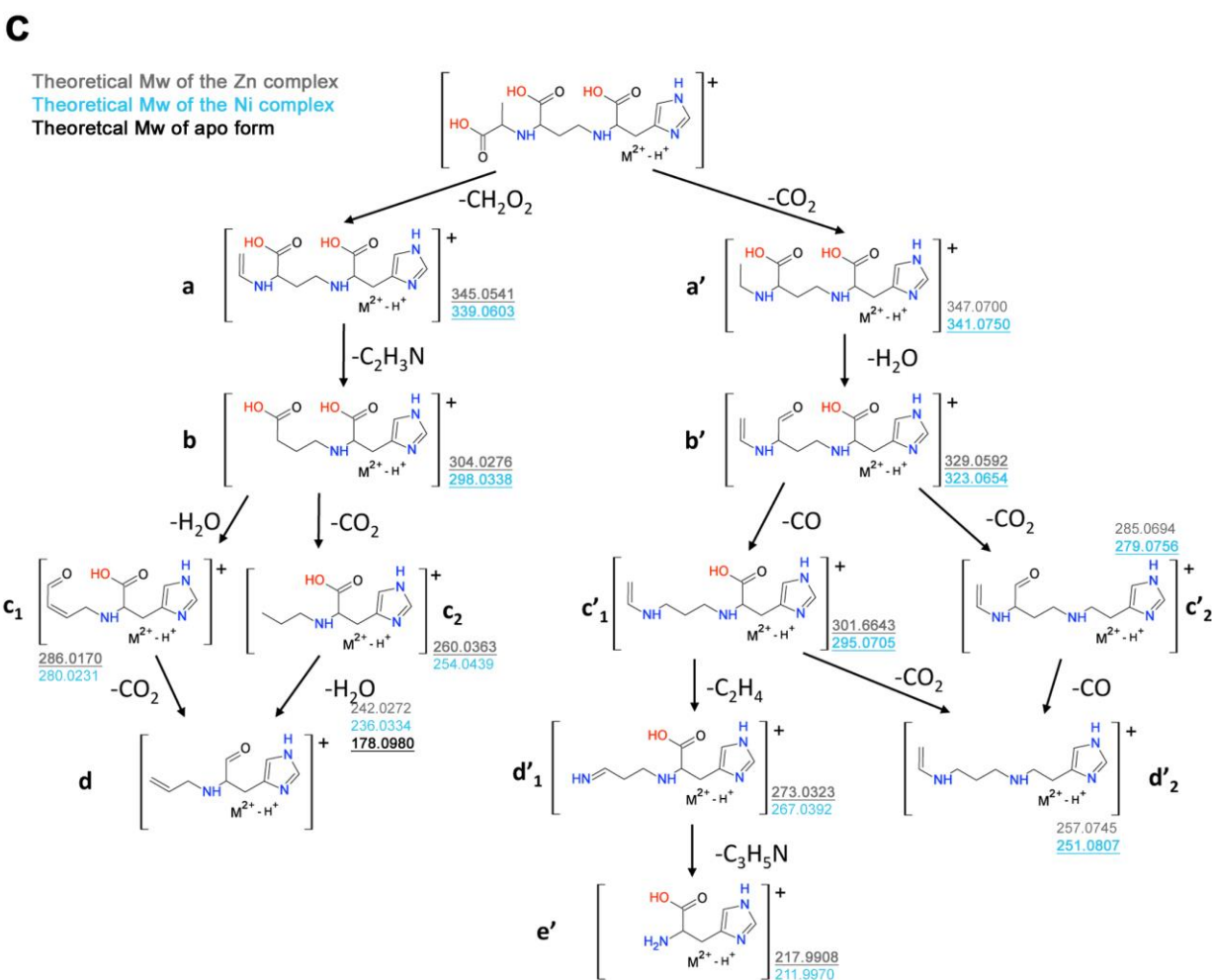
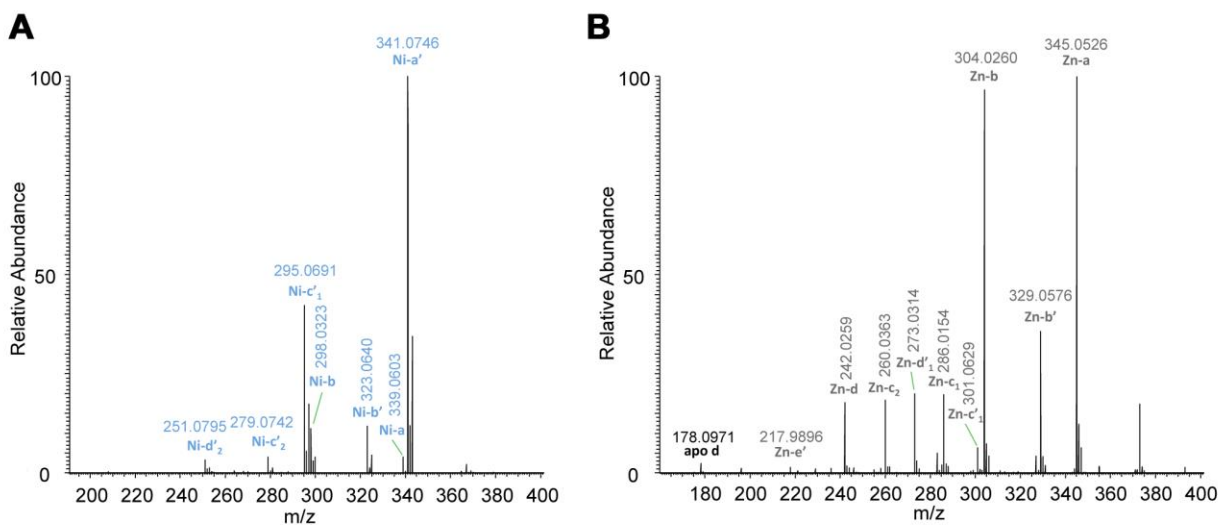


B



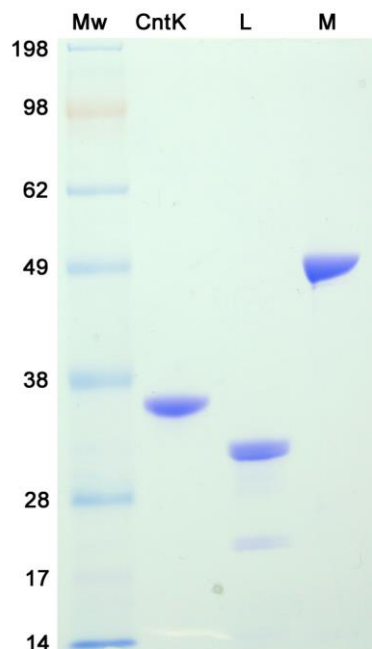
1
2
3
4
5
6
7

Figure S4: Fishing of the metallophore through a knowledge based approach. (A) Scheme of the “knowledge based approach”. (B) Final mass spectra of CntA after incubation and re-purification.

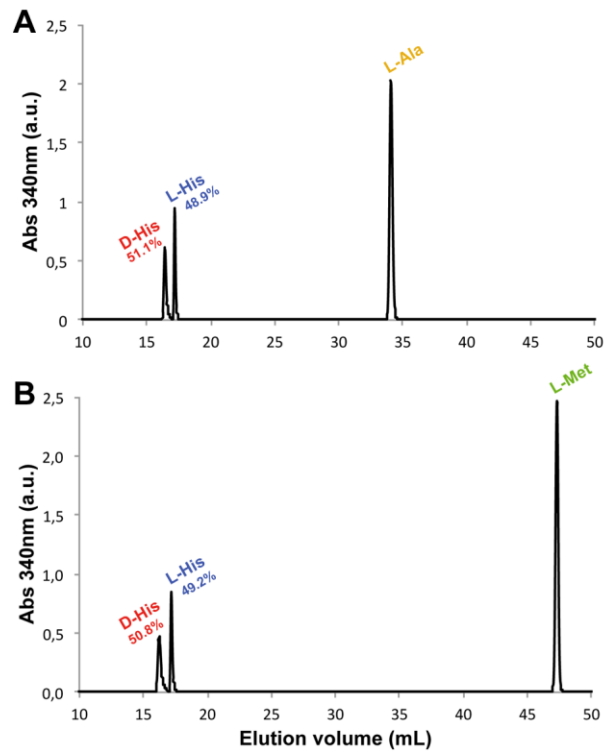


1
 2 **Figure S5: MS/MS fragmentation of Staphylopine-Metal complexes.** MS/MS fragmentation
 3 of Staphylopine-Zn (A) and Staphylopine-Ni complexes (B). The mass of the ions are indicated
 4 as well as their interpretation with the fragmentation scheme shown in (C). (C) Proposed

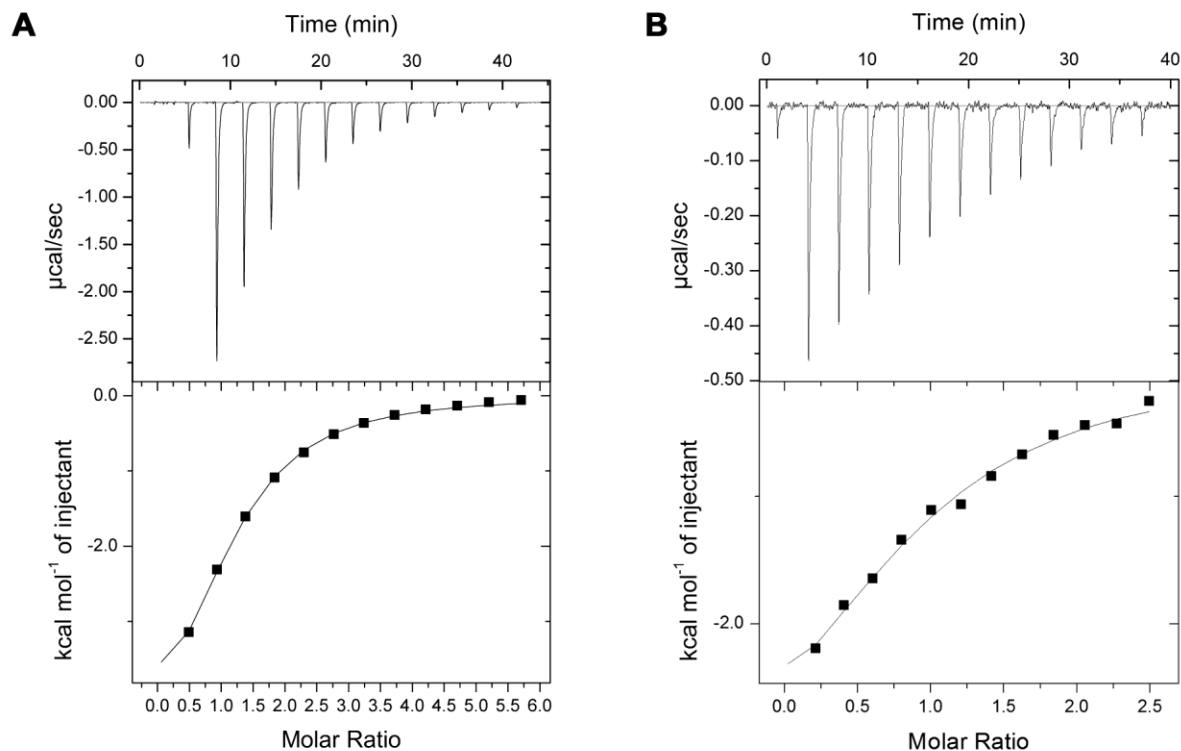
1 fragmentation scheme of Staphylopine-Zn and Staphylopine-Ni complexes. The theoretical
2 masses of the ions are indicated on the right of the proposed ion. The underlined masses were
3 detected in the observed fragmentation pattern shown in (A) and (B).
4



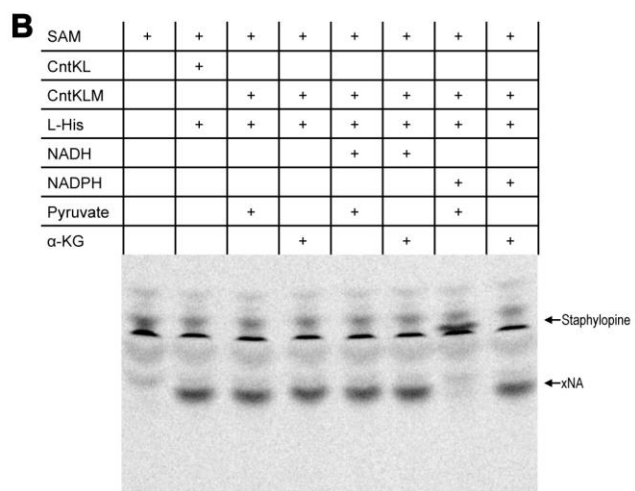
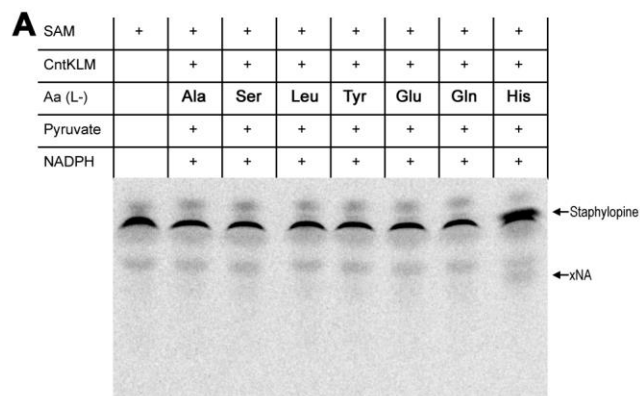
1
2 **Figure S6: SDS-PAGE gel of purified CntK, CntL and CntM.** The expected molecular
3 weights are 35 kDa, 31 kDa and 51kDa for CntK, CntL and CntM respectively. The final
4 purification yields are 2, 5 and 20 mg of pure protein per liter of culture.
5



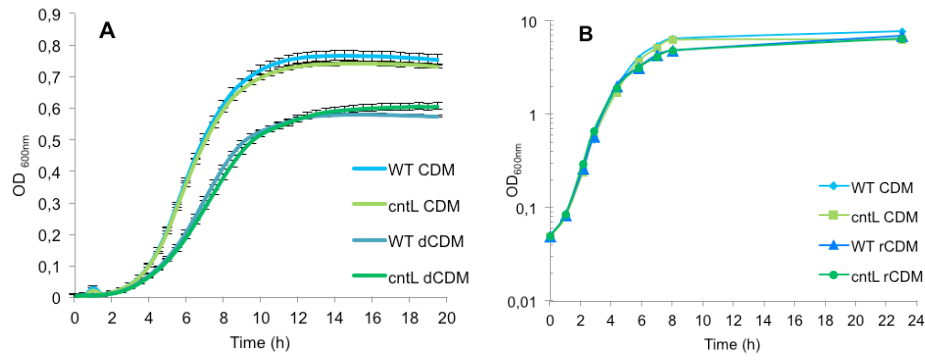
1
 2 **Figure S7: Activity of CntK in the presence of competing amino acids.** (A) CntK was
 3 incubated with 20 mM of L-histidine and 40 mM of L-alanine. (B) CntK was incubated with 20
 4 mM of L-histidine and 40 mM of L-methionine.



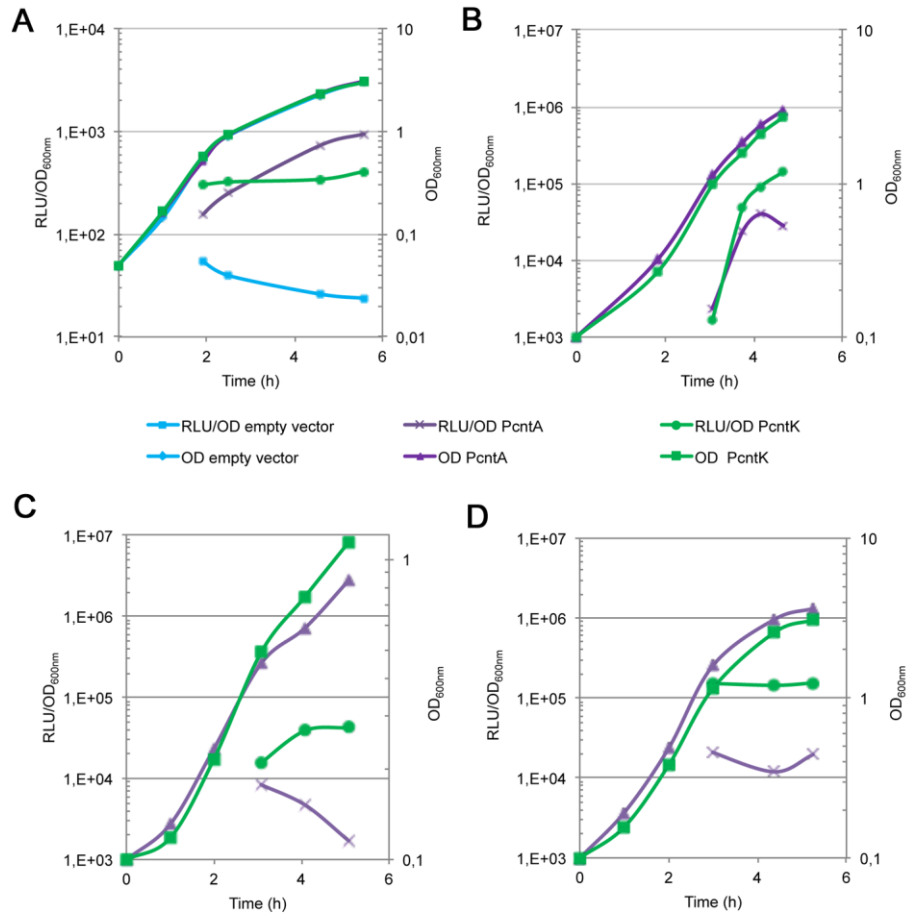
1
 2 **Figure S8: Microcalorimetric titration of CntL with SAM and CntM with NADPH.** (A)
 3 Representative data (raw data on top and curve fit below) from an ITC experiment where SAM
 4 was titrated into the reaction cell containing CntL. The first addition (not used in the fit) was half
 5 the volume of the other additions. Thermodynamic values obtained from the curve fit are: $\Delta S =$
 6 1.29 cal/mol/K , $\Delta H = -5212 \pm 211.5 \text{ cal/mol}$, $K_d = 68 \pm 5 \text{ }\mu\text{M}$, $n = 1.07 \pm 0.03$, where n is the
 7 stoichiometry of the binding. (B) Representative data (raw data on top and curve fit below) from
 8 an ITC experiment where NADPH was titrated into the reaction cell containing CntM. The first
 9 addition (not used in the fit) was half the volume of the other additions. Thermodynamic values
 10 obtained from the curve fit are: $\Delta S = 6.91 \text{ cal/mol/K}$, $\Delta H = -3831 \pm 530.1 \text{ cal/mol}$, $K_d = 48 \pm 4$
 11 μM , $n = 0.929 \pm 0.09$, where n is the stoichiometry of the binding.
 12



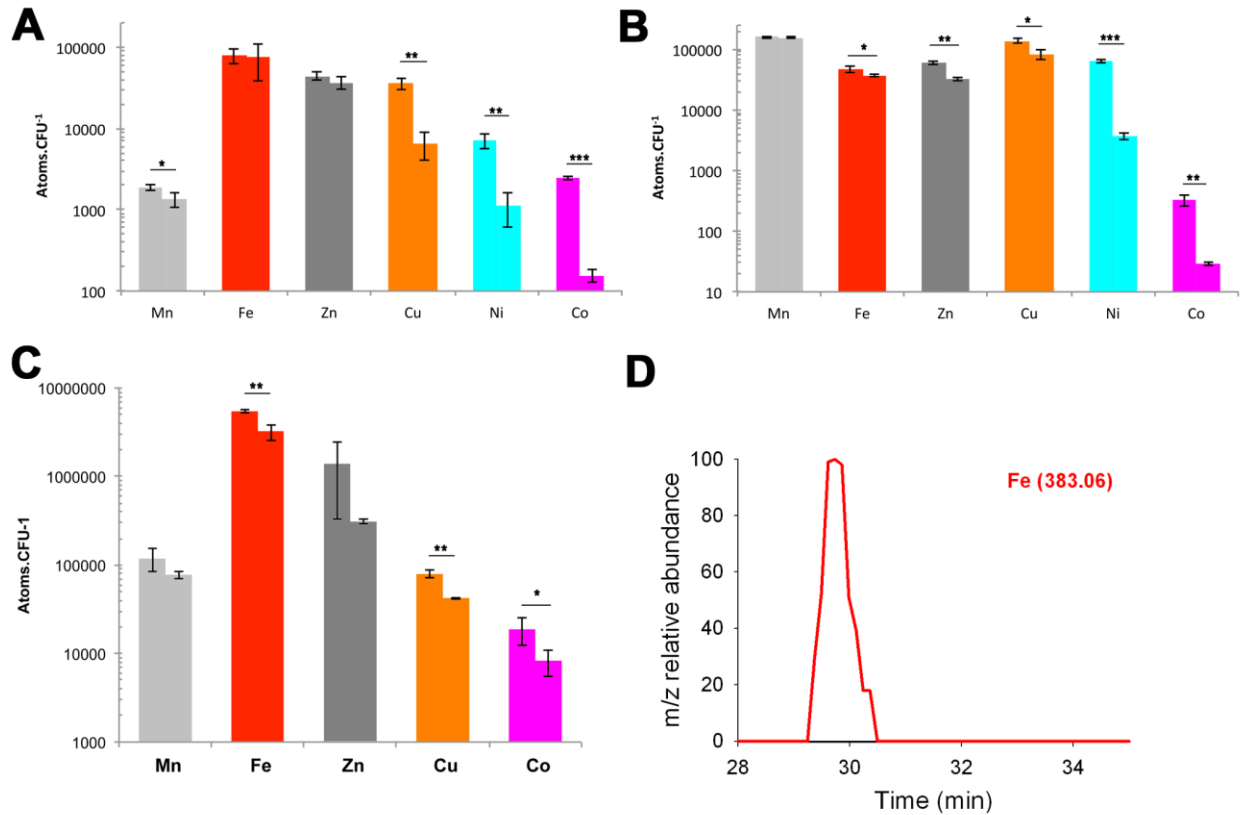
1
 2 **Figure S9: Substrate specificity of CntK, CntL and CntM.** (A) Test of seven different L-
 3 aminoacids with divers properties on the activity of CntKLM using NADPH and pyruvate as
 4 substrates of CntM. (B) Test of substrate specificity of CntM using all three biosynthetic
 5 enzymes and different CntM substrates (NADPH vs NADH and pyruvate vs α -keto glutarate; α -
 6 KG).
 7



1
 2 **Figure S10: Growth curves of the WT and *cntL* strains of *S. aureus*.** (A) in CDM and
 3 demetalated CDM (dCDM) in microplates, or (B) in CDM and demetalated-NTA CDM with
 4 metalated NTA resin (rCDM) in 50 ml tubes at 37°C with aeration.
 5



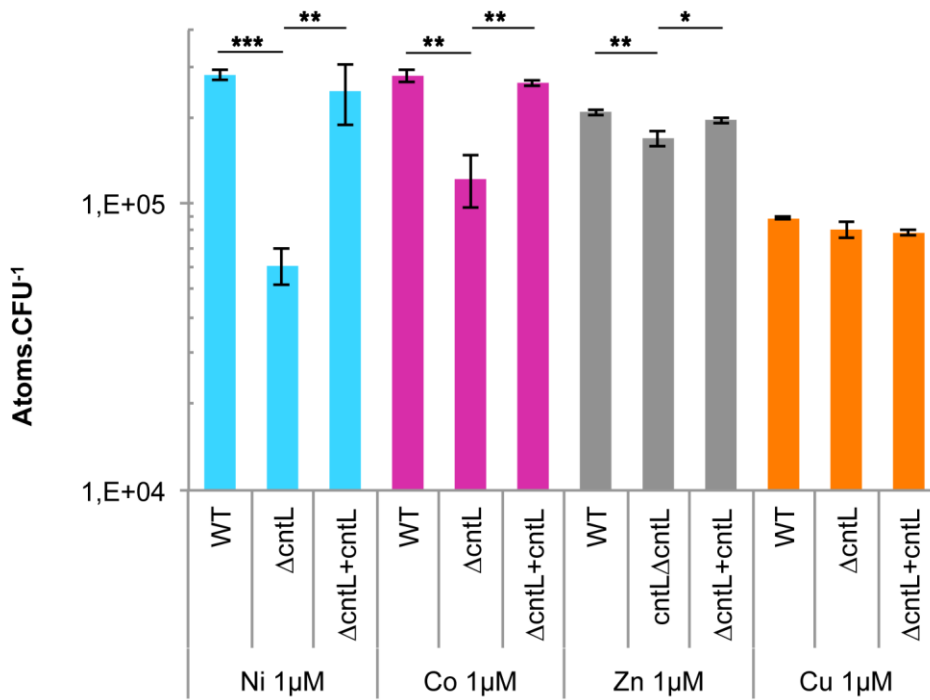
1
 2 **Figure S11: Luciferase activities of WT strain harbouring fusion of *PcntA-luxAB* (PcntA)**
 3 **and *PcntK-luxAB* (PcntK) in various media. (A) LB medium. (B) CDM. (C) dCDM. (D)**
 4 **rCDM.**



1
2 **Figure S12: Import of divalent metals in various culture conditions.** (A) Intracellular metal
3 content determined by ICP-MS of *S. aureus* WT (left bars) and *cntL* (right bars) mutant strains
4 grown in dCDM. Error bars, mean \pm s.d. * $P < 0.05$ and ** $P < 0.01$. (B) Intracellular metal content
5 determined by ICP-MS of *S. aureus* WT (left bars) and *cntL* (right bars) mutant strains grown in
6 rCDM. Error bars, mean \pm s.d. * $P < 0.05$, ** $P < 0.01$ and *** $P < 0.001$. (C) Intracellular metal
7 content determined by ICP-AES of *S. aureus* WT (left bars) and *cntL* (right bars) mutant strains
8 grown in LB medium without further metal supplementation. Error bars, mean \pm s.d. * $P < 0.05$
9 and ** $P < 0.01$. (D) HILIC/ESI-MS extracted ion chromatograms (XIC) of the Staphylopin-Fe
10 complex detected in the extracellular fraction of *S. aureus* grown in CDM. Chromatogram was
11 traced using the exact mass of the complex (± 3 ppm). This mass was absent in the extracellular
12 fraction of the *cntL* mutant.

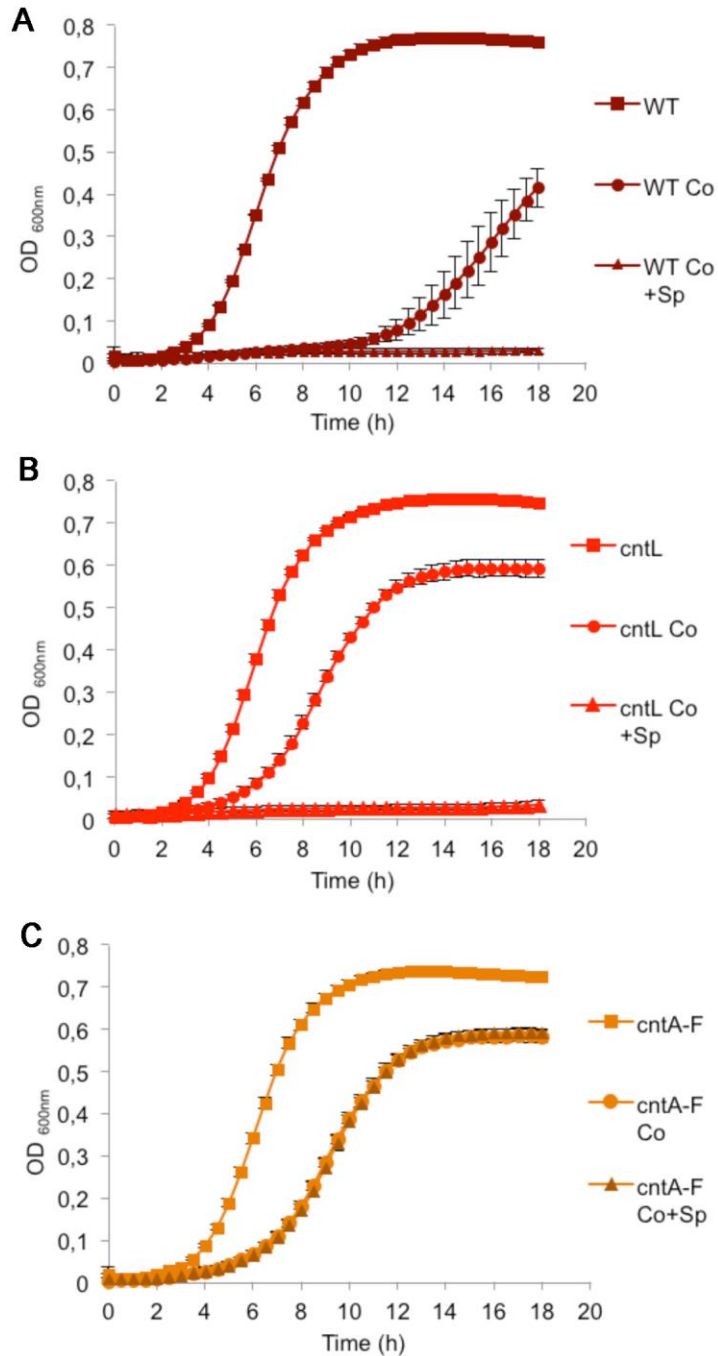
13

1

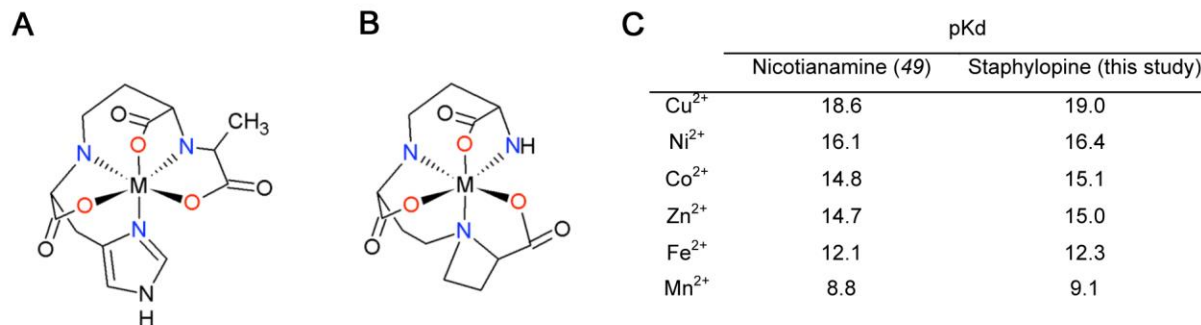


2

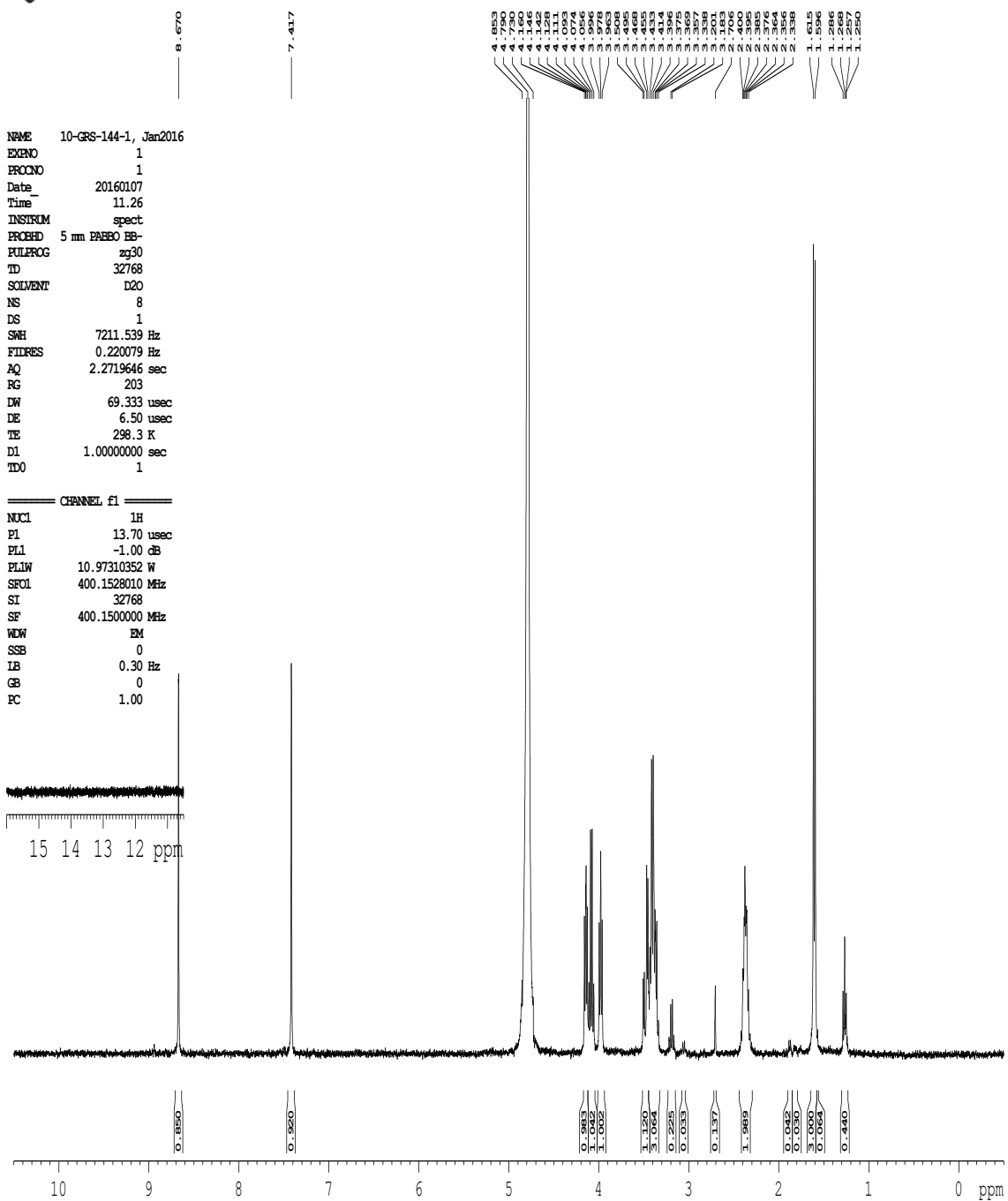
3 **Figure S13: Metal content of WT *S. aureus*, *cntL* mutant and complemented strains.** Cells
4 were grown in CDM supplemented with the indicated metal (1 μ M), and subsequently grown
5 overnight, prior to determination of their intracellular metal concentration by ICP-AES. Error
6 bars, mean \pm s.d. ** P <0.01 and *** P <0.001.



1
 2 **Figure S14: Toxicity of cobalt and CntA-F / staphylopin-dependent transport of cobalt.**
 3 (A) WT, (B) *cntL* and (C) *cntA-F* strains were grown at 37°C in microplates in CDM
 4 supplemented or not with 2mM cobalt (Co), 10µM of staphylopin (Sp), or both (Co+Sp).
 5 Growth in CDM +/- Sp alone was similar for all strains, indicating that staphylopin alone is not
 6 toxic or beneficial in these conditions.



1
 2 **Figure S15: Putative structure and estimated pKd for staphylopin by comparison with**
 3 **nicotianamine.** Putative chemical structure of staphylopin-metal complex (**A**) and
 4 nicotianamine-metal complex (**B**). (**C**) pKd values for staphylopin complexes were estimated by
 5 metal competition experiments with nicotianamine by ESI MS.
 6



1
 2 **Figure S16: NMR spectrum of synthetic staphylopine.**

Name	Sequence (5'-3')	Targeted plasmid
CntA-Fw	CACCATGAGAAAATACTAAATG	pET100
CntA-Rv	TTATTTATACTGCATTTTCATTGAA	
CntK-Fw	CACCATGAATCGGCAGGTTATAGA	pET100
CntK-Rv	TTATTCTATATATGCTTTTCCTGT	
CntL-Fw	AATAACTTTAATAATGAAATCAA	pET SUMO
CntL-Rv	TTAGACATCCGTAATACCTACCTTTATA	
CntM-Fw	CACCATGTCTAAATTATTAATGATAGGCAC	pET101
CntM-Rv	TGAAAGCGTTCTATTGATTTCCA	
Cntop-Fw	AGAAGGAGATATACATATGAATCGGCAGGTTATAG AATTTTCT	pET22b+
Cntop-Rv	GGTGGTGGTGCTCGAGAAGACTACTCGCTGGACGT GGTGTT	
Mut-cntL5'A	CGGGATCCTGGCCGCAACACATGTATGCTGTG	pMAD
Mut-cntL3'A	CATCCGTAATACCTACAAAGTTATTCATTGTAGGCT CCTTATTC	pMAD
Mut-cntL5'B	TACAATGAATAACTTTGTAGGTATTACGGATGTCTA AAT	pMAD
Mut-cntL3'B	CGGGATCCGCTAAAGCAGAGATTCGTTGACAC	pMAD
Mut-cntE-5'A	CGCGGATCCTGTTGGAAGAAGTCGGTCTATC	pMAD
Mut-cntE-3'A	ACTACTCGCTCAAGCCATTGCACCTTTCAT	pMAD
Mut-cntE-5'B	GCAATGGCTTCAGCGAGTAGTCTTTAATGAAGT	pMAD
Mut-cntE-3'B	TCCCCCGGGTAATACATGGTGGGAATTCATTCC	pMAD
pOS-cntL5	CGCGGATCCGCCTACAATGAATAACTTTAATAATG	pOS1-Plgt
pOS-cntL3	CGCGGATCCGGATTGCGACCGGACCAGTGC	pOS1-Plgt
pLUX-cntK5	CGCGGATCCGAAGTTTATGGAAGGATTATC	pCN58
pLUX-cntK3	CCGGAATTCCGACACTCCTTTAGATGTA	pCN58

1 **Table S1: Oligonucleotides used in this study**

2

3

4

Ingredient	Final medium concentration (g/l)
D-glucose	4
Amino acids	
L-cysteine	0,48
L-aspartic acid	2,4
L-glutamic acid	2,4
L-proline	2,4
L-arginine	0,36
L-glycine	2,4
L-histidine	0,48
L-lysine HCL	0,6
L-serine	2,4
L-valine	0,48
L-threonine	2,4
L-alanine	2,4
L-isoleucine	0,6
L-leucine	0,6
L-tryptophan	0,06
L-methionine	0,18
L-tyrosine	0,18
L-phenylalanine	0,2
Salts	
Na ₂ HPO ₄	5,7
(NH ₄) ₂ SO ₄	6,84
KH ₂ PO ₄	1,34
MgSO ₄ 7H ₂ O	0,247
Vitamins	
Nicotinic acid	0,01194
Thiamine HCL	0,0006
Ca panthothenate	0,002
Biotine	0,0001

1 **Table S2: Composition of chemically defined medium.** The pH is adjusted to 7 with KOH and
2 the volume to 1L with milliQ water. The medium is then sterilized by filtration through a
3 0,22µm filter.

	Culture media concentration, nM					
	Mn	Fe	Zn	Cu	Ni	Co
LB	116 ± 9	4450 ± 356	5320 ± 426	206 ± 16	25 ± 2	134 ± 11
CDM	17 ± 3	171 ± 14	105 ± 8	7 ± 2	12 ± 2	< 5
dCDM	< 5	20 ± 3	22 ± 3	< 5	< 5	< 5

1
2 **Table S3: Metal concentrations in culture media and in the intracellular fraction of WT**
3 **cells in different culture conditions.**

1 **Supplementary references**

- 2 34. S. F. Altschul *et al.*, *Nucleic Acids Res* **25**, 3389 (1997).
3 35. R. D. Finn *et al.*, *Nucleic Acids Res* **42**, D222 (2014).
4 36. R. C. Edgar, *Nucleic Acids Res* **32**, 1792 (2004).
5 37. M. Clamp, J. Cuff, S. M. Searle, G. J. Barton, *Bioinformatics* **20**, 426 (2004).
6 38. L. A. Kelley, S. Mezulis, C. M. Yates, M. N. Wass, M. J. Sternberg, *Nat Protoc* **10**, 845
7 (2009).
8 39. D. Vallenet *et al.*, *Nucleic Acids Res* **41**, D636 (2013).
9 40. A. Hiron, E. Borezee-Durant, J. C. Piard, V. Juillard, *J Bacteriol* **189**, 5119 (2007).
10 41. M. Arnaud, A. Chastanet, M. Debarbouille, *Appl Environ Microbiol* **70**, 6887 (2004).
11 42. C. Rigoulay *et al.*, *Infect Immun* **73**, 563 (2005).
12 43. J. Bubeck Wardenburg, W. A. Williams, D. Missiakas, *Proc Natl Acad Sci U S A* **103**,
13 13831 (2006).
14 44. D. Taylor, K. T. Holland, *J Appl Bacteriol* **66**, 319 (1989).
15 45. L. Grillet *et al.*, *J Biol Chem* **289**, 2515 (2014).
16 46. L. Ouerdane, S. Mari, P. Czernic, M. Lebrun, R. Lobinski, *Journal of Analytical Atomic*
17 *Spectrometry* **21**, 676 (2006).
18 47. N. von Wiren *et al.*, *Plant Physiol* **119**, 1107 (1999).
19 48. K. Higuchi, K. Kanazawa, N. K. Nishizawa, S. Mori, *Plant and Soil* **178**, 171 (1996).
20 49. I. Benes, S. K., H. Ripperger, A. Kircheiss, *Experientia* **39**, 261 (1983).

21